

## Accepted Manuscript

Synthesis, crystal structure, spectroscopic analysis and computational study of (Z)-1-(2, 4-dinitrophenyl)-2-((E)-3-(4-methoxyphenyl)-1-(thiophen-2-yl) allylidene) hydrazine by DFT and AIM approach

Ashok Kumar Singh, Ravindra Kumar Singh

PII: S0022-2860(15)00114-3

DOI: <http://dx.doi.org/10.1016/j.molstruc.2015.02.029>

Reference: MOLSTR 21327

To appear in: *Journal of Molecular Structure*

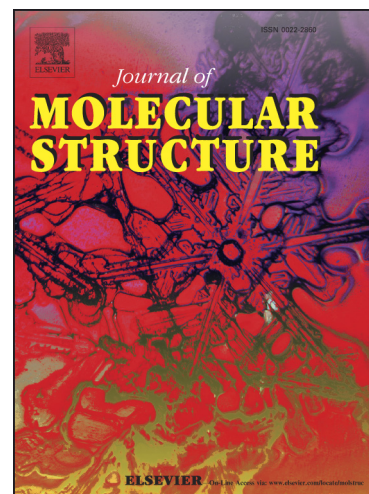
Received Date: 10 December 2014

Revised Date: 5 February 2015

Accepted Date: 9 February 2015

Please cite this article as: A.K. Singh, R.K. Singh, Synthesis, crystal structure, spectroscopic analysis and computational study of (Z)-1-(2, 4-dinitrophenyl)-2-((E)-3-(4-methoxyphenyl)-1-(thiophen-2-yl) allylidene) hydrazine by DFT and AIM approach, *Journal of Molecular Structure* (2015), doi: <http://dx.doi.org/10.1016/j.molstruc.2015.02.029>

This is a PDF file of an unedited manuscript that has been accepted for publication. As a service to our customers we are providing this early version of the manuscript. The manuscript will undergo copyediting, typesetting, and review of the resulting proof before it is published in its final form. Please note that during the production process errors may be discovered which could affect the content, and all legal disclaimers that apply to the journal pertain.



Synthesis, crystal structure, spectroscopic analysis and computational study of (Z)-1-(2,4-dinitrophenyl)-2-((E)-3-(4-methoxyphenyl)-1-(thiophen-2-yl) allylidene) hydrazine by DFT and AIM approach

Ashok Kumar Singh\*, Ravindra Kumar Singh

Department of Chemistry, University of Lucknow, Lucknow 226 007, India

#### ABSTRACT

The title compound was synthesized and characterized by IR,  $^1\text{H}$  NMR,  $^{13}\text{C}$  NMR and single crystal X-ray diffraction studies. Quantum chemical calculations have been performed at DFT level of theory using B3LYP functional and 6-31G (d, p) as basis set. Potential energy distribution (PED) for the normal modes of vibrations was done using Gar2ped program. The time dependent density functional theory (TD-DFT) was used to find the various electronic transitions within molecule in two different solvent of varying polarity. Non linear optical (NLO) behavior of title compound was investigated in different solvents by the computed value of first hyperpolarizability ( $\beta_0$ ). A combined theoretical and experimental correlation of  $^1\text{H}$  and  $^{13}\text{C}$  NMR spectra are in good agreement. Stability of molecules as a result of hyper-conjugative interactions and electron delocalization were analyzed using NBO analysis. The HOMO and LUMO analysis is used to determine the charge transfer within the molecule. Intramolecular interactions were analyzed by AIM approach. The chemical reactivity descriptors were calculated to study the reactive sites within molecule.

**Keywords:** Hydrazone; XRD; TD-DFT; Hyperpolarizability; NBO analysis; AIM approach

\*Corresponding Authors: Cell: +91-9919663856

E-mail address: [singhaks3@rediffmail.com](mailto:singhaks3@rediffmail.com) (A.K. Singh)

## Introduction

Hydrazones are an important class of compounds due to their various properties and applications. Hydrazones having frame  $\text{—C=N—NH—}$  constitute an important class of compounds for [2 + 2] cycloadditions, 1, 3 dipolar cycloadditions and have been turned into a valuable tool for the synthesis of azetidiones, pyrazoles, respectively [1, 2] and various other N, O or S containing heterocyclic compounds such as oxadiazolines, thiazolidinones and triazolines [3-7]. They constitute an important class of compounds for new drug development. They are used as antimicrobial, anti-tubercular [8-11] and anti-diabetic agents [12]. They have strong coordinating ability towards different metal ions [13, 14]. In addition, aroyl hydrazones and their mode of chelation with transition metal ions present in the living system have been of significant interest [15, 16]. The chemical stability of hydrazones and their high melting point have recently made them attractive as prospective new material for optoelectronic applications [17]. Phenyl hydrazones exhibit a series of good organic non-linear optical (NLO) properties [18, 19].

Since most organic molecules forms molecular crystals in which the molecules are held together by weak Van der Waals interactions, their macroscopic properties can roughly be estimated from the microscopic properties of individual molecules. So, quantum chemical calculations on a single molecule are useful tool not only in reproducing experimental results but also in predicting properties of new materials. The discovery that conjugated organic materials can exhibit large non-linear optical properties has triggered large scale theoretical and experimental investigation in this area [20, 21]. The organic compounds showing high hyperpolarizability are those containing an electron donating group or an electron withdrawing group interacting through a system of conjugated double bonds.

In the present paper we report the synthesis, crystal and optimised structure along interactions involved using quantum chemical calculations and AIM approach. Furthermore, quantum

chemical calculations are also performed to analyze the molecular structure, spectral analysis, various intra-molecular interactions and chemical reactivity of the titled compound. AIM approach has extensively been applied to classify and understand hydrogen bonding interactions and ellipticity in the synthesized molecule. Local reactivity descriptors were calculated to study the reactive site within the molecule.

## Experimental

### Material and methods

All experiments were carried out in under ambient atmosphere. All chemicals used were of analytical grade. The solvent was purified and dried according to standard procedures (A.I. Vogel, Practical Organic Chemistry). Thin layer chromatography (TLC) was performed on Silica Gel 'G' (Merck, India) coated plates for monitoring the progress of reaction. The chalcone (E)-3-(4-methoxy phenyl)-1-(thiophen-2-yl)prop-2-en-1-one was synthesized by base catalyzed Claisen-Schmidt condensation reaction, by an earlier reported methods [22]. Melting points ( $^{\circ}\text{C}$ ) were determined in an open capillary by electro-thermal melting point apparatus and were uncorrected. Elemental analysis (C, H, N, and S) was performed on Varian Elementar – III analyzer. Infrared (IR) spectra were recorded in KBr pellets on Perkin Elmer FTIR RX-1 spectrometer from  $4000\text{-}450\text{ cm}^{-1}$ .  $^1\text{H}$  nuclear magnetic resonance (NMR) spectrum of synthesized compound was recorded in  $\text{CDCl}_3$  on Bruker DRX-300 MHz and  $^{13}\text{C}$  NMR Spectra was recorded on JOEL AL 300 FTNMR (75MHz) using (TMS) as internal reference. Coupling constants  $J$  are expressed in Hertz (Hz). UV/Visible spectra were taken on LABTRONICS LT2900 spectrophotometer equipped with a 1.0 cm quartz cell.

### Synthesis

To a stirred and hot solution of (E)-3-(4-methoxyphenyl)-1-(thiophen-2-yl)prop-2-en-1-one (5 mmol) added a hot ( $50\text{-}60^{\circ}\text{C}$ ) acidic solution of 2,4-dinitrophenyl hydrazine, prepared by careful addition of concentrated sulphuric acid (1.5 mL ) to suspension of 2,4-dinitrophenyl

hydrazine (1g, 5.05 mmol ) in methanol (15 mL).The hot mixture was stirred for 5-10 min. and then refluxed for about 3h and then allowed to cool at room temperature. The precipitated hydrazone was filtered and washed with 0.01M sulphuric acid, followed by cold ether. The crude solid was purified by recrystallization from alcohol to give purified compound. The compound was confirmed for its purity by melting point, elemental analysis and other spectral studies. Scarlet red powder, Yield: 1.75g, 79%, Mp: 164-166 °C, Anal. Calcd for  $C_{20}H_{16}N_4O_5S$  (424.43) C, 56.60; H, 3.80; N, 13.20; S, 7.55. Found C, 56.76; H, 3.63; N, 13.08; S, 7.34%. Synthetic scheme for preparation of hydrazone compound is shown in Fig.1.

**Fig. 1**

#### X-ray crystallography

The crystal of X-ray quality for the compound was obtained by slow evaporation of ethanol/diethyl ether solvent mixture at room temperature. X-ray crystallographic data was recorded by mounting single reddish brown crystal of compound of size (0.300 x 0.220 x 0.200) mm<sup>3</sup> on glass fibers. Cell determination and intensity data were collected at 298(2) K on a Oxford diffraction XCALIBUR-S CCD area detector diffractometer system equipped with graphite monochromated Mo K $\alpha$  radiation  $\lambda = 0.71073 \text{ \AA}$ . The final unit cell determination, scaling of data and correction for Lorentz and polarization effects were performed. Symmetry related (multi-scan) absorption correction has been applied. Structure solution by direct methods, followed by full matrix least square refinement technique on  $F^2$  using anisotropic displacement parameters, was performed using the WINGX v 2013.3 suite [23] and SHELX-97 programs [24]. All non-hydrogen atoms were refined anisotropically; hydrogen atoms were located at calculated positions and refined using riding model. Figure was prepared using ORTEP-3 [25]. Summary of crystallographic data is presented in Table 1.

**Table 1**

## Computational details

The molecular geometry optimization and all quantum-chemical calculations have been performed with Gaussian 09 program package [26] using DFT- B3LYP functional with the 6-31G(d, p) basis set. The  $^1\text{H}$  NMR and  $^{13}\text{C}$  NMR chemical shifts were calculated by employing Gauge Induced atomic orbital (GIAO) method [27]. A newly designed functional, the long range Coulomb attenuating method (CAM-B3LYP) comprising of 81% of B88 exchange at short-range and 65% of HF plus 35% of B88 at long-range [28], has been applied and was reasonably capable of predicting the excitation energies and absorption spectra of the D- $\pi$ -A molecules having charge-transfer excitations [29-31]. The energies and intensities of the 30 lowest energy spin allowed electronic excitations were computed with the help of TD-DFT using CAM-B3LYP method in vacuum and also in solvents using polarized continuum model (PCM) [32]. The solvents parameters used were dichloromethane and ethanol. Using the optimized coordinates of the compound, the first static hyperpolarizability ( $\beta_0$ ) was calculated employing the finite field perturbation method in vacuum as well as in the solvents having differing polarity using PCM model [32]. Stability of molecules as a result of hyper-conjugative interactions and electron delocalization were analyzed using natural bond orbital (NBO) analysis [33]. Potential energy distribution along internal coordinates is calculated by Gar2ped software [34]. Internal coordinate system recommended by Pulay et al. is used for the assignment of vibrational modes [35]. Presentation graphics including molecular geometries visualizations were done using Gauss view 5.0 [36] program. The wave function obtained from the optimization was used to calculate the topological parameters at the BCPs using the Bader's theory of 'Atoms in Molecules, implemented in AIM 2000 software [37].

## Results and discussion

### Chemistry

According to the literature, hydrazones may exist as *Z/E* geometrical isomers about C=C bond of ethylene bridge and about C=N bond of hydrazone moiety [38]. The synthesized hydrazones is found to be in *E*-configuration with respect to -HC=CH-. This is confirmed by presence of two, <sup>1</sup>H doublet with coupling constant *J* in range of 16.0-16.5 Hz [39]. The presence of distinct medium band at 974cm<sup>-1</sup> is due to C-H out of plane bending of trans disubstituted alkenes [40]. Due to possibility of different arrangement of substituent with respect to -C=NH-, the existence of two isomers are possible. Such steric structural changes are well reflected in NMR spectra as two set of resonance in low field region. In the 300MHz, <sup>1</sup>H NMR (in CDCl<sub>3</sub>) spectra of compound paired peak for each proton of DNP ring and -HN-N=, corresponding to (*E*) - and (*Z*) - forms of compounds with respect to C=N were clearly observed. The intensities of paired peak differed from other, due to variable amount of *E/Z* isomers, which are usually unequal. Two signals for N-H protons were found to be present at δ11.67 and δ11.43 ppm. The relative integration for the two signals indicates that yield % of (*Z*)- and (*E*)-isomers for compound is found to be 40.33% and 37.67%. The (*Z*)-isomer was found to be somewhat more in comparison to (*E*)-isomer. This may be due to extra stabilization of (*Z*) - isomer by intra-molecular N-H...O hydrogen bond.

Although the product hydrazone was found to be as (*EE*) - and (*EZ*)-isomeric mixture, but the solid state crystal structure obtained is for predominating and more stable (*EZ*)-isomer. So, all the quantum calculations, have been performed for isomer (*Z*)-1-(2, 4-dinitrophenyl)-2-((*E*)-3-(4-methoxyphenyl)-1-(thiophen-2-yl) allylidene) hydrazine.

### Crystal structure description

The ORTEP view of the title compound is shown in Fig. 2. The crystal structure of compound shows that the molecule crystallises in triclinic system having space group P-1. The asymmetric unit of compound was found to contain two molecules. The unit cell packing is found to contain four molecules. The molecular structure is non-planar. The compound exists in *E*-configuration with respect to their C8-C9 double bond with bond distance of 1.326 Å. The compound exists in *Z*-configuration with respect to their C=N double bond with bond distance of 1.302 Å. The two phenyl ring A and B are almost planar with dihedral angle of 2.04°-1.12°. The thiophene ring (Th) is somewhat perpendicular to ring A and B in order to relieve the H...H steric strains. For unit I dihedral angle between DNP ring Ph<sub>2</sub> and Th ring is found to be 36.80° and between methoxy phenyl ring Ph<sub>1</sub> and Th ring is 57.72° and for unit II dihedral angle between ring Ph<sub>2</sub> and Th ring is found to be 43.92° and between ring Ph<sub>1</sub> and Th ring is 54.84°.

**Fig. 2**

The analyses of X-ray crystal structure reveals the presence of several interactions. As seen from the packing diagram of the unit cell, two asymmetric units interact with other units by intermolecular H-bonds, as shown in Supplementary material (S Fig.1). Overall, interactions results in supramolecular architecture of molecule expanding in cyclic dimeric manner, producing three dimensional multilayered patterns. Hydrogen bonds geometry is shown in Table 2.

**Table 2**

### Thermodynamic properties

Thermodynamic quantities were calculated, applying vibrational frequency calculations for all reactants and products at room temperature (298.15 K). The enthalpy ( $\Delta H_{\text{Reaction}}$ ), Gibbs

free energy ( $\Delta G_{\text{Reaction}}$ ) and entropy change of reaction ( $\Delta S_{\text{Reaction}}$ ) were calculated and arranged in Table 3. Reactants: 3-(4-methoxyphenyl)-1-(thiophen-2-yl) prop-2-en-1-one and 2, 4-dinitro phenyl hydrazine, products titled hydrazone and water (as byproduct) were abbreviated as **1**, **2**, **3**, and **4** respectively. For overall reaction, the enthalpy change ( $\Delta H_{\text{Reaction}}$ ), Gibbs free energy change ( $\Delta G_{\text{Reaction}}$ ) and entropy change ( $\Delta S_{\text{Reaction}}$ ) are calculated to be 1.1923, 3.0120 kcal/ mol and 5.906 cal/mol K, respectively. The positive values for  $\Delta H$  and  $\Delta G$  indicates that the reaction is endothermic and non-spontaneous at room temperature. The reaction becomes spontaneous at elevated temperature and the temperature gap will reduce in presence of catalyst (weak acid). Using thermodynamic relation, equilibrium constant ( $K_{\text{eq}}$ ) for the title reaction is calculated as  $6.183 \times 10^{-3}$  at room temperature. Therefore, reaction is not favored in the forward direction at room temperature and confirms the formation of product **3** at high temperature. Therefore refluxing condition is required for the reaction.

**Table 3**

#### Optimized geometry

The optimized molecular structure of (Z)-1-(2, 4-dinitrophenyl)-2-((E)-3-(4-methoxyphenyl)-1-(thiophen-2-yl) allylidene) hydrazine (**3**) was determined using Gaussian 09 program. The geometrical parameters of crystal structure of synthesized compound are taken for optimization of structure. Optimized molecular structure has C1 symmetry with energy of -1764.854 au. Comparison between selected optimized geometrical parameters at B3LYP/6-31G (d, p) with experimental X-ray crystallographic parameters is given in Table 4. Optimized geometrical structure of compound is shown in Fig.3.

**Table 4****Fig. 3**

From the table, the elongation of C–C bond length of C4–C5 (1.4308 Å) and C4–C11 (1.4218 Å) than that of C5–C10 (1.3956 Å), C13–C14 (1.4056 Å) is because of the delocalization of electron density of phenyl ring with the nitro groups. The aromatic ring of the title compound is somewhat irregular and the spread of CC bond distance is 1.3825–1.4132 Å in Ph<sub>1</sub> and 1.3810–1.4308 Å in Ph<sub>2</sub>, which is similar to the spread reported by Smith et al. [41]. Nitro group is highly electronegative and tries to obtain additional electron density of the benzene ring. It attempts to draw it from the neighboring atoms, which move closer together, in order to share the remaining electrons more easily as a result, due to this the bond angle, A(10,13,14) is found to be 121°, and A(4,5,10) is found to be 121.1° in the present calculation, which is 120° for normal benzene. The C–H bond lengths in rings Ph<sub>1</sub> and Ph<sub>2</sub> of the title compound lie respectively, between 1.083–1.085 Å and 1.081–1.082 Å. The calculated bond length and bond angles of thiophene ring are in good agreement with the experimental as well as with earlier reported value for such compounds.

Chambers et al. [42] reported the N–O bond lengths in the range 1.2201–1.2441 Å, C–N length as 1.4544 Å. For the title compound, the C–N (NO<sub>2</sub>) bond lengths are 1.4528, 1.4591 Å and N–O bond lengths are in the range 1.2288–1.2466 Å, which are in agreement with the reported values. The C–N–O angles are reported [43] in the range 117.4–118.7°, where as for the title compound it is in range 117.4–118.7°. The bond angles of the NO<sub>2</sub> group of the title compound O17–N23–O29 = 122.8°, O29–N23–C5=118.7°, O17–N23–C5=118.5° and O16–N20–O26 = 124.7° , O16–N20–C13 =117.4°, O26–N20–C13=117.9° are in agreement with the values 123.5, 118.7, and 117.9° given by Saeed et al. [44].

The calculated C4–N3 bond distance of 1.3608 Å indicates that C–N bond shows partial double bond character in this fragment. Also C–N bond length are found to be much shorter than the average value for a single C–N bond (1.47Å), but significant longer than a C=N double bond (1.22Å) [45], suggesting the presence of multiple bond character. The C=C bond

length is 1.3535Å and C–C bond lengths lie in the range 1.4843–1.4582Å which is in agreement with reported literature[46]. Espinoza-Hicks et.al [47] has reported O–C<sub>aromatic</sub> and O–CH<sub>3</sub> bond length as 1.365Å and 1.428Å. In the present case, the respective bond lengths are 1.3598 and 1.4213 Å.

When the X-ray structure of the title compound is compared with its optimized counterpart conformational discrepancies are observed. Some discrepancies are observed in the orientation of two phenyl rings and thiophene ring, which is defined by dihedral angle C21–C9–C4–C12 = 2.02° (Ph<sub>1</sub> and Ph<sub>2</sub>), C15–C9–C24–S1 = 57.72° (Ph<sub>1</sub> and Th) and C5–C4–C24–C25=36.8° (Ph<sub>2</sub> and Th). These dihedral angles have been calculated at 2.02°, 58.45° and 45.81°. When the geometry of hydrogen bond in the optimized is examined, the proton donor group N3–H31 forms intra-molecular interaction with O17 atom, with bond length of 1.8574° and a bond angle of 128.9° for calculated B3LYP. The N3—H31 involved in intra-molecular H-bond are found to be 1.021Å (exp.0.884Å) and 1.021Å (exp.0.846Å) respectively. Major discrepancy of about 5.5° in bond angle of N2—N3—H31 and 4.8° in bond angle of C4—C3—H31 was observed. The discrepancies between the XRD results and the calculated geometrical parameters are due to fact that the comparison made between experimental data, obtained from solid state single crystal and calculated results are for isolated molecule in gaseous state.

In spite of the differences, calculated geometric parameters represent a good approximation and they are the basis for calculating other parameters, such as vibrational frequencies, electronic absorption spectra, molecular electrostatic parameters and other optical and spectroscopic properties.

#### IR spectra and vibrational assignments

The observed and calculated (scaled) vibrational wave numbers at B3LYP/6-31G (d, p) level and their assignments using PED are given in Table 5. The calculated IR spectrum in the

region 4000–400  $\text{cm}^{-1}$  is shown graphically in Fig. 4. The experimental IR spectrum is shown in Supplementary material (S Fig. 2). The total number of atoms in compound is 46, which give 132 ( $3n-6$ ) vibrational modes. The calculated vibrational wave numbers are higher than their experimental values for the majority of the normal modes. The calculated wave numbers are scaled down using single scaling factor 0.9608 to discard of any harmonicity present in real system [48]. The correlation graph is shown in Fig. 5. The value of correlation coefficient found to be  $r = 0.999$ , showing good agreement with the calculated wave numbers with experimental. The potential energy distribution (PED) and modes obtained from Gauss-View program help in the assignment of the calculated harmonic vibrational wave numbers and peaks of experimental FT-IR spectrum.

**Table 5**

**Fig. 4**

**Fig. 5**

C—N and N—H vibrations

In the IR spectrum of compound, two bands for C—N stretching vibration were observed, one between aromatic carbon and nitrogen of sec. amine and other between aromatic ring carbon and nitrogen of nitro group. Stretching vibration for C4—N3 was observed at 1489  $\text{cm}^{-1}$ , showing good agreement with the calculated wave number at 1492  $\text{cm}^{-1}$ . Stretching vibration for C5—N23 and C13—N20 for two nitro groups was observed at 912  $\text{cm}^{-1}$ , shows good agreement with the calculated wave number at 908  $\text{cm}^{-1}$ . The N—H stretching vibrations generally give rise bands [49] at 3500-3300  $\text{cm}^{-1}$ . In the present study, the N-H stretch of carbohydrazide part (—C=N—NH—) of molecule is observed at 3258  $\text{cm}^{-1}$ , whereas it is calculated at 3311  $\text{cm}^{-1}$ . The N—H stretching frequency is red shifted by 53  $\text{cm}^{-1}$  in the IR spectrum with a strong intensity from the computed frequency, which indicates the weakening of the N—H bond due to the elongation of conventional hydrogen bond donor (N-

H bond) than the hydrogen bond free N—H group resulting in intra-molecular hydrogen bond with the neighboring oxygen atom of nitro group [50]. Besides this N—H bending vibration for secondary amine and N—H wagging vibration were observed at 1421 and 694  $\text{cm}^{-1}$  showing good agreement with the calculated wave number at 1419 and 699  $\text{cm}^{-1}$  respectively.

#### NO<sub>2</sub> vibrations

The most characteristic bands in the spectra of nitro compounds are due to NO<sub>2</sub> stretching vibrations. The molecule under investigation possesses two nitro groups, and hence one expects a symmetric and asymmetric vibration. In Aromatic nitro compounds symmetric and asymmetric N=O stretching bands occur at slightly lower wave number than nitro-alkanes due to conjugation with phenyl ring. Asymmetric stretching vibrations are always observed at higher wave number than symmetric stretching vibrations. In nitro compounds NO<sub>2</sub> stretching vibrations are located in the regions 1550–1300  $\text{cm}^{-1}$ [51]. Nitrobenzene derivatives display  $\nu_{\text{as}}\text{NO}_2$  in the region  $1535 \pm 30 \text{ cm}^{-1}$  and 3-nitropyridines at  $1530 \pm 10 \text{ cm}^{-1}$ [52] and in substituted nitrobenzene [53]  $\nu_{\text{as}}\text{NO}_2$  appears strongly at  $1345 \pm 30 \text{ cm}^{-1}$  and in conjugated nitro-alkenes [53] at  $1345 \pm 15 \text{ cm}^{-1}$ . For the title compound, calculations give asymmetric stretching vibrations of (N=O) at 1588 and 1556  $\text{cm}^{-1}$ , where as experimental was found to be at 1588  $\text{cm}^{-1}$ . Symmetric stretching vibrations was observed at 1331 and 1309  $\text{cm}^{-1}$ , where as calculated was found to be 1329 and 1309  $\text{cm}^{-1}$  respectively. For nitrobenzene,  $\delta_{\text{sc}}\text{-NO}_2$  is reported [54] at 852  $\text{cm}^{-1}$  and for 1, 3-dinitrobenzene at 904 and 834  $\text{cm}^{-1}$ . For the title compound, this band was observed at 815  $\text{cm}^{-1}$  and was calculated to be at 823  $\text{cm}^{-1}$ . In aromatic compounds, the wagging mode  $\omega\text{NO}_2$  is expected in the region  $740 \pm 50 \text{ cm}^{-1}$  with a moderate to strong intensity [54]. The  $\omega\text{NO}_2$  is reported at 701 and 728  $\text{cm}^{-1}$  for 1, 2-dinitrobenzene and at 710 and 772  $\text{cm}^{-1}$  for 1, 4-dinitrobenzene [54]. For the title compound, the band at 732  $\text{cm}^{-1}$  in the IR spectrum is assigned as  $\omega\text{NO}_2$  mode, which shows good

agreement with the calculated value at  $732\text{cm}^{-1}$ . The rocking mode  $\rho\text{NO}_2$  is active in the region  $540 \pm 70\text{ cm}^{-1}$  in aromatic nitro compounds [54]. This  $\rho\text{NO}_2$  mode was calculated to be at  $507\text{ cm}^{-1}$ . Varsanyi et al. [55] and Suryanarayana et al. [56] reported the ranges  $70 \pm 20$  and  $65 \pm 10\text{ cm}^{-1}$  respectively, as the torsion mode of  $\tau\text{NO}_2$  for aromatic compounds. In the present case, the deformation modes of  $\text{NO}_2$  are calculated to be present at  $65$  and  $56\text{ cm}^{-1}$ .

#### C=N and C=C vibrations

The observed C=N stretching vibration at  $1511\text{ cm}^{-1}$  agrees well with the calculated wave number which lies in region  $1536\text{--}1516\text{ cm}^{-1}$ . The C=C stretching vibration of olefinic bond was observed at  $1616\text{ cm}^{-1}$ . The calculated wave number at  $1618\text{ cm}^{-1}$  was assigned to the stretching vibration mode of olefin present at C12—C7. In aromatic hydrocarbon, skeletal vibrations involving carbon—carbon stretching within ring are absorbed mainly in region  $1604$  and  $1409\text{ cm}^{-1}$ . The wave number calculated at  $1605\text{ cm}^{-1}$  and  $1419\text{ cm}^{-1}$  was assigned to the C=C stretches in benzene ring whereas experimentally it is observed at  $1605\text{ cm}^{-1}$ ,  $1489\text{ cm}^{-1}$  and  $1421\text{ cm}^{-1}$  respectively. The wave number calculated at  $1516\text{ cm}^{-1}$  was assigned to the C=C stretches in thiophene ring, shows good agreement with the calculated wave number at  $1511\text{ cm}^{-1}$ .

#### C—H vibrations

According to internal coordinate system recommended by Pulay et al. [57], methyl (Me) group associate with 5 types of vibrational frequencies namely: symmetric stretch, asymmetric stretch, symmetric deformation, asymmetric deformation and rocking. The observed stretching vibration of ether methyl (C—O—Me) at  $3029$ ,  $2934$  and  $2901\text{ cm}^{-1}$  is in agreement with the calculated wave number at  $3032$ ,  $2965$  and  $2903\text{ cm}^{-1}$  respectively. An asymmetric deformation of Me (C30) is observed at  $1464$  and  $1447\text{ cm}^{-1}$  whereas the calculated value found as merged peak at  $1458\text{ cm}^{-1}$ . Symmetric deformation of  $\text{—CH}_3$  is observed at  $1428\text{ cm}^{-1}$ , whereas the calculated is found to be at  $1430\text{ cm}^{-1}$ . The observed

methyl (C30) rocking at  $1175\text{ cm}^{-1}$ , agrees well with the calculated wave number at  $1164\text{ cm}^{-1}$ . The aromatic and olefinic structure in this molecule shows the presence of C—H stretching vibration in the region  $3142\text{--}3050\text{ cm}^{-1}$ , which is the characteristic region for the identification of C—H stretching vibration [58]. The experimental spectra show only two medium-weak band at  $3102$  and  $3086\text{ cm}^{-1}$ . Most prominent band of C—H out-of-plane (“oop”) bending for aromatic rings, occurs in low frequency range between  $968\text{--}689\text{ cm}^{-1}$ . The C-H, out-of-plane bending vibrations for olefinic was observed at  $974\text{ cm}^{-1}$  was assigned to trans disubstituted alkene  $C(7)=C(12)$ , shows good agreement with the calculated value at  $966\text{ cm}^{-1}$ .

#### C—O and C—S vibrations

In the molecule methoxy group is present at C18 as  $\text{CH}_3\text{—O6—C18}$  ether linkage. The presence of aryl alkyl ether displays stretching band at  $1264\text{ cm}^{-1}$ , shows good agreement with the calculated value at  $1261\text{ cm}^{-1}$ . Symmetrical C—O stretching was observed at  $1027\text{ cm}^{-1}$ , where as calculated was found to be  $1030\text{ cm}^{-1}$ . The C—S stretching vibration for C24—S1 and C28—S1 of thiophene ring was observed at  $732\text{ cm}^{-1}$  and  $573\text{ cm}^{-1}$ , was in agreement with the theoretical value at  $722\text{ cm}^{-1}$  and  $573\text{ cm}^{-1}$ .

#### $^1\text{H}$ and $^{13}\text{C}$ NMR spectra

The  $^1\text{H}$  and  $^{13}\text{C}$  NMR chemical shifts of are calculated with GIAO approach using B3LYP method and 6-31G (d, p) basis set [59]. Chemical shift of any atom (X) is calculated as difference between isotropic magnetic shielding (IMS) of TMS and atom (X). It is defined by an equation written as:  $\delta_X = \text{IMS}_{\text{TMS}} - \text{IMS}_X$ .

The experimental and calculated values of  $^1\text{H}$  and  $^{13}\text{C}$  NMR chemical shifts of the title compound are given in Table 6. The experimental  $^1\text{H}$  and  $^{13}\text{C}$  NMR spectra are shown in Supplementary material (S Figs. 3 and 4). In order to compare the chemical shifts correlation, graphics between the experimental and calculated  $^1\text{H}$  NMR chemical shifts are shown in Fig.

6. The correlation graph follow the linear equation ( $y = 0.940x + 0.423$ ); where  $y$  is the experimental  $^1\text{H}$  NMR chemical shift,  $x$  is the calculated  $^1\text{H}$  NMR chemical shift (in ppm). The value of correlation coefficient ( $R^2 = 0.993$ ) shows that there is a good agreement between experimental and calculated results. The correlation between the experimental and the calculated  $^{13}\text{C}$  NMR chemical shifts of compound is given in Fig.7. The correlation graph follow the linear equation ( $y = 0.837x + 17.32$ ); where  $y$  is the experimental  $^{13}\text{C}$  NMR chemical shift,  $x$  is the calculated  $^{13}\text{C}$  NMR chemical shift (in ppm). The graph shows good correlation between the experimental and the calculated results with the coefficient of regression  $R^2 = 0.995$ .

**Table 6**

**Fig. 6**

**Fig. 7**

UV–Visible spectroscopy

To obtain the nature of electronic transitions, electronic excitation energies and oscillatory strength, the UV–visible spectrum of compound has been studied by TD-DFT using CAM-B3LYP method. The TD-DFT excitations were calculated both on the gas phase and in the solvent using the IEF-PCM model (ethanol and dichloromethane). Experimental UV–Vis spectrum of compound **3** in both solvents is shown in Fig. 8. The calculated electronic spectra in gas phase and both the solvents are shown as Supplementary material (S Figs.5, 6 and 7).

As seen from the calculated spectra in solvent phase, two distinct absorption bands are found in UV-region with  $\lambda$  max at 382 nm arising from H(110)  $\rightarrow$  L(111) electronic transition and  $\lambda$  max at 215 nm arising due to electronic transition from H-3(107)  $\rightarrow$  L(111) molecular orbitals. These bands are observed in experimental spectrum at 421 and 219 nm in DCM and at 417 and 217 nm in solvent ethanol. The strong intensity band calculated at 382nm ( $f =$

1.12-1.09) can be assigned to an intramolecular charge transfer (ITC) between donating and acceptor fragments through charge transfer axis. By comparing the calculated spectra in two solvents of different polarity, it is evident that calculated transitions do not exhibit solvatochromic effects. The observed and calculated electronic transitions of high oscillatory strength and their assignments, along with experimental wavelength in gas phase, ethanol and DCM are presented in Table 7. However, in comparison to the gas phase spectrum, the bands observed displays significant red shifting of 5 -18 nm in solvent dichloromethane and ethanol. The experimental wavelength at 421 and 417 nm in DCM and ethanol shows significant hyperchromic shift (red shift) in comparison to the calculated values at 382 nm. The hyperchromic shift is occurring due to hydrogen bonding of the solvent effect. The calculated electronic excitations give rise to the same pattern of bands, at energies and are in good agreements with the experimental spectrum. The main difference between the experimental and TD-DFT spectra arises from the relative intensities of the peaks observed at 215 nm in UV region. On the basis of calculated molecular orbital coefficients analysis and molecular orbital plots for the title compound, the FMOs are mainly composed of *p*-atomic orbital's and so the nature of major electronic excitations are assigned to be  $\pi \rightarrow \pi^*$ .

**Fig. 8**

**Table 7**

Frontier molecular orbitals

The energy gap between the HOMO and LUMO is a critical parameter in determining molecular electrical transport properties because it is a measure of electron conductivity [60].

Frontier molecular orbital's HOMO and LUMO as well as other molecular orbitals involved in electronic transitions, along their energy obtained from TD-DFT/CAM-B3LYP calculation using PCM model for compound **3** in solvent dichloromethane are shown in Fig. 9. The

HOMOs are the orbital that could act as electron donor and the LUMOs are the orbital that could act as electron acceptor [61]. As seen from MO's plot, HOMO is mainly centered on methoxy phenyl ring (which act as donor fragment) whereas LUMO is mainly located over dinitro phenyl ring (which act as acceptor fragment). The HOMO–LUMO energy gap is an important stability index and reflects the chemical stability of the molecule.

HOMO energy = -5.5783 eV

LUMO energy = -2.5578 eV

HOMO—LUMO energy gap = -3.0205 eV

**Fig. 9**

Molecular electrostatic potential (MEP)

The MEP is related to the electron density and is very useful descriptor in determining the sites for electrophilic and nucleophilic reactions as well as hydrogen bonding interactions [62, 63]. The electrostatic potential  $V(r)$  is also well suited for analyzing processes based on the recognition of one molecule by another, as in drug-receptor and enzyme-substrate interactions [64]. Being a real physical property,  $V(r)$  can be determined experimentally by diffraction or by computational methods. Electrostatic potential correlates with dipole moment, electronegativity, partial charges and site of chemical reactivity of the molecule. It provides a visual method to understand the relative polarity of a molecule. The negative electrostatic potential corresponds to an attraction of the proton by the concentrated electron density in the molecule (colored in shades of red on the ESP surface), the positive electrostatic potential corresponds to repulsion of the proton by atomic nuclei in regions where low electron density exists and the nuclear charge is incompletely shielded (colored shades of blue). The different values of electrostatic potential at the surface are represented by different colors as red represents the region of most electronegative electrostatic potential,

blue represents region of most positive electrostatic potential and green represents region of zero potential. Potential increases in the order red < orange < yellow < green < blue.

To predict reactive sites for electrophilic and nucleophilic attack for the investigated molecule, the MEP at the B3LYP/6-31G (d, p) optimized geometry was calculated. The electron density isosurface on to which the electrostatic potential surface has been mapped is shown in Fig. 10. The negative (red and yellow) regions of MEP were related to electrophilic reactivity and the positive (blue) regions to nucleophilic reactivity. From the MEP it is evident that the negative charge covers the nitro group and oxygen atom of methoxy group and the positive region is mainly over the methyl group. These sites give information about region where the compound can have intermolecular interactions.

**Fig. 10**

NBO analysis

NBO analysis has an appealing aspect of highlighting the individual bonds and lone-pair energy that play a vital role in the chemical processes [65, 66]. It is an important tool for studying hybridization, covalence, hydrogen-bonding and Vander Waals interactions. In other words natural bond orbital (NBO) provides supplementary structural information. The higher value of  $E^{(2)}$  (stabilization energy or energy of hyper conjugative interaction) points toward the greater interaction between electron donors and electron acceptors (i.e. the more donating tendency from electron donors to electron acceptors and the greater the extent of conjugation in the system). For each donor NBO ( $i$ ) and acceptor NBO ( $j$ ), the strength of interaction (or stabilization energy)  $E^{(2)}$  associated with electron delocalization between donor and acceptor is estimated by the second order energy lowering as [67]

$$E^{(2)} = \Delta E_{ij} = q_i \frac{(F_{ij})^2}{(\epsilon_j - \epsilon_i)}$$

Where,  $q_i$  is the population of donor orbital or donor orbital occupancy;  $\epsilon_i$ ,  $\epsilon_j$  are orbital energies (diagonal elements) of donor and acceptor NBO orbitals respectively;  $F_{ij}$  is the off-diagonal Fock or Kohn–Sham matrix element between  $i$  and  $j$  NBO orbitals.

Second-order perturbation theory analysis for selected donor (Lewis) and acceptor (non-Lewis) orbital's, of the Fock matrix in NBO basis calculated at B3LYP/6-31G (d,p) is presented in Table 8, which shows  $\pi$ -conjugation/resonance due to  $\pi$ -electron delocalization in aromatic rings, primary and secondary hyper-conjugative interactions. The  $\pi$ -conjugation/resonance due to  $\pi$ -electron delocalization is involved due to the  $\pi$ - $\pi^*$  interactions whereas, the primary hyper conjugative interactions due to the various types of orbital overlaps such as  $\sigma$ - $\pi^*$ ,  $\pi$ - $\sigma^*$   $n$ - $\sigma^*$  and secondary hyper conjugative interactions due to the orbital overlap  $\sigma$ - $\sigma^*$ . Delocalization of electron density between occupied Lewis-type (bonding or lone pair) NBO's and unoccupied (antibonding) non-Lewis NBO's corresponds to a stabilizing donor-acceptor interactions.

The hyper-conjugative interactions of  $\pi$  (C9-C15)  $\rightarrow$   $\pi^*$ (C21-C22)/ $\pi^*$ (C18-C19),  $\pi$  (C18-C19)  $\rightarrow$   $\pi^*$ (C21-C22)/ $\pi^*$ (C9-C15),  $\pi$ (C21-C22)  $\rightarrow$   $\pi^*$ (C18-C19)/ $\pi^*$ (C9-C15) are responsible for conjugation of respective  $\pi$  bonds in methoxy phenyl (Ph<sub>1</sub>) ring and interaction of  $\pi$  (C9-C15)  $\rightarrow$   $\pi^*$ (C7-C12) with extended C(7)=C(12) bond. The electron density (ED) at the conjugation of  $\pi$  bonds (1.63424-1.72423) of ring Ph<sub>1</sub> and  $\pi^*$  bonds (0.16263-0.39185) of ring Ph<sub>1</sub> indicates strong  $\pi$  delocalization within the ring and with conjugated olefinic bond leading stabilization energy in range of 22.78-16.15 kcal/mol. The interactions  $\pi$  (C5-C10) and  $\pi$  (C11-C14) of di-nitro phenyl (Ph<sub>2</sub>) ring with NO<sub>2</sub> and -NH substituent's of ring viz.  $\pi$ (C5-C10)  $\rightarrow$   $\pi^*$ (N3-C4)/ $\pi^*$ (N23-O29) and  $\pi$ (C11-C14)  $\rightarrow$   $\pi^*$ (N3-C4) stabilizes Ph<sub>2</sub> ring by energy in the region of 32.70-30.89 kcal/mol. The  $\pi \rightarrow \pi^*$  interactions viz.  $\pi$  (C24-C25)  $\rightarrow$   $\pi^*$ (C27-C28) and  $\pi$  (C27-C28)  $\rightarrow$   $\pi^*$ (C24-C25) are responsible for delocalization of respective  $\pi$ -electrons of thiophene ring, stabilizing the molecule in the region 16.13-14.74-

15.3 kcal/mol. The interactions of the conjugated system outside the rings viz.  $\pi$  (N2-C8)  $\rightarrow$   $\pi^*$ (C7-C12),  $\pi$  (C7-C12)  $\rightarrow$   $\pi^*$ (C27-C28)/ $\pi^*$ (C27-C28) and  $\pi^*$ (N3-C4)  $\rightarrow$   $\pi^*$ (N2-C8) are also stabilizing the molecule up to 19.88-10.88 kcal/mol. The charge transfer interactions are formed by the orbital overlap between bonding ( $\pi$ ) and antibonding ( $\pi^*$ ) orbitals, which results in intramolecular charge transfer (ICT) causing stabilization of the system. The movement of  $\pi$ -electron cloud from donor to acceptor i.e. intramolecular charge transfer (ICT) can make the molecule more polarized and the ICT must be responsible for the NLO properties of molecule. Therefore, the titled compound may be used for non-linear optical materials application in future.

The primary hyper conjugative interactions  $n \rightarrow \sigma^*$  responsible for weak intra-molecular interactions between N3-H31...O17 (Intra-molecular H-bond) is from  $n_1$  (O17)  $\rightarrow$   $\sigma^*$ (N3-H31) and  $n_2$  (O17)  $\rightarrow$   $\sigma^*$ (N3-H31) which increases ED (0.06208) that weakens the respective bond leading to stabilization in range of 8.56-4.60 kcal/mol. The increased electron density at the nitrogen atom (N3) leads to the elongation of respective bond length and a lowering of corresponding stretching wave number. Other high energy interaction involving lone pair of electron with antibonding  $\pi$  electrons are  $n_2$  (S1)  $\rightarrow$   $\pi^*$ (C24-C25) and  $n_2$  (S1)  $\rightarrow$   $\pi^*$ (C27-C28) which increases ED (0.28211-0.32309) that weakens the respective bond leading to stabilization within the range of 21.56-20.53 kcal/mol. The hyper conjugative interaction  $n_2$  (O6)  $\rightarrow$   $\pi^*$ (C18-C19) indicates the delocalization of lone pair of electrons on oxygen atom of  $-\text{OCH}_3$  group with antibonding  $\pi$  electrons of phenyl ring, which increases ED (0.39185) that weakens the respective bond leading with stabilization energy of 32.21 kcal/mol. Various secondary hyper-conjugative interactions ( $\sigma \rightarrow \sigma^*$ ) are also associated with the molecule which stabilizes the molecule maximum up to 5.13 kcal/mol. The hyper conjugative interaction energy was deduced from the second-order perturbation approach. The NBO

analysis also describes the bonding in terms of natural hybrid orbital. The results are tabulated in Supplementary material (S Table 1).

### Table 8

#### Chemical Reactivity

#### Global reactivity descriptors

The chemical reactivity and site selectivity of the molecular systems have been determined by the conceptual density functional theory [68]. Electronegativity ( $\chi$ ), chemical potential ( $\mu$ ), global hardness ( $\eta$ ), global softness ( $S$ ) and electrophilicity index ( $\omega$ ) are global reactivity descriptors, highly successful in predicting global reactivity trends. On the basis of *Koopman's theorem* [69], global reactivity descriptors are calculated using the energies of frontier molecular orbital's HOMO and LUMO.

According to Parr et al., electrophilicity index ( $\omega$ ) [70] is a global reactivity index similar to the chemical hardness and chemical potential. This is positive and definite quantity. This new reactivity index measures the stabilization in energy when the system acquires an additional electronic charge ( $\Delta N$ ) from the environment. The direction of the charge transfer is completely determined by the electronic chemical potential of the molecule because an electrophile is a chemical species capable of accepting electrons from the environments; its energy must decrease upon accepting electronic charge. Therefore its electronic chemical potential must be negative. The energies of frontier molecular orbitals ( $E_{\text{HOMO}}$ ,  $E_{\text{LUMO}}$ ), energy band gap ( $E_{\text{HOMO}}-E_{\text{LUMO}}$ ), electro negativity ( $\chi$ ), chemical potential ( $\mu$ ), global hardness ( $\eta$ ), global softness ( $S$ ) and global electrophilicity index ( $\omega$ ) for **1**, **2** and **3** are listed in Table 9.

### Table 9

When two molecules react, which one will act as an electrophile (nucleophile) will depend upon higher (lower) value of electrophilicity index. The high value of electrophilicity index shows that product **(3)** is stronger electrophile than reactants **1**. Electrophilic charge transfer (ECT) is defined as the difference between the  $\Delta N$  max values of interacting molecules. If we consider two molecules **1** and **2** approach to each other (i) if  $ECT > 0$ , charge flows from **2** to **1** (ii) if  $ECT < 0$ , charge flows from **1** to **2**. ECT is calculated using equation  $ECT = (\Delta N \max)_1 - (\Delta N \max)_2$ , where  $(\Delta N \max)_1 = (\mu/\eta)_1$  and  $(\Delta N \max)_2 = (\mu/\eta)_2$ . ECT is calculated as -0.3455 for reactant molecules **1** and **2**, which strongly indicates that charge flows from molecule **1** to **2**. Therefore, **1** acts as very strong electron donor and **2** as electron acceptor. The high value of chemical potential and low value of electrophilicity index ( $\omega = 4.031$  eV) for **1** favor its strong nucleophilic behavior. In the same way, the low value of chemical potential and high value of electrophilicity index ( $\omega=5.656$  eV) for **2** favor its electrophilic behavior.

#### Local reactivity descriptors

Fukui function is one of the widely used local density functional descriptors to model chemical reactivity and selectivity. Local reactivity descriptors such as local softness ( $S_k$ ), Fukui function ( $f_k$ ) and local electrophilicity index ( $\omega_k$ ) [71] have been used in DFT theory for defining the reactive site within a particular molecule. Fukui function  $f(r)$  is considered as one of the most fundamental indicator for defining the site selectivity in a given molecular species and soft-soft type of interactions, the preferred reactive site in a molecule is the one with maximum values of ( $f_k, S_k, \omega_k$ ) [72]. Using Hirshfeld atomic charges of neutral, cation and anion state of reactant **(1)**, reactant **(2)** and product **(3)** Fukui functions ( $f_k^+, f_k^-, f_k^0$ ), local softnesses ( $s_k^+, s_k^-, s_k^0$ ) and local electrophilicity indices ( $\omega_k^+, \omega_k^-, \omega_k^0$ ) were calculated.

Fukui functions, local softnesses and local electrophilicity indices for selected atomic sites in reactant **(1)**, reactant **(2)** and product **(3)** using Hirshfeld atomic charges have been listed in

Table 10. The maximum values of all the three local electrophilic reactivity descriptors ( $f_k^+$ ,  $s_k^+$ ,  $\omega_k^+$ ) at C-9 position of reactant (1) indicate that this site is prone to nucleophilic attack. Using Hirshfeld atomic charges, the maximum values of local electrophilic reactivity descriptors ( $f_k^-$ ,  $s_k^-$ ,  $\omega_k^-$ ) at C-9 for reactant (1) and the maximum values of local nucleophilic reactivity descriptors ( $f_k^-$ ,  $s_k^-, \omega_k^-$ ) at N-18 for reactant (2) confirms the formation of product molecule (3) i.e. Schiff base linkage (C8=N2) of hydrazone. The maximum values of local electrophilic reactivity descriptors ( $f_k^+$ ,  $s_k^+$ ,  $\omega_k^+$ ) at carbon (C-8) for (3) indicate that this site is more prone to nucleophilic attack and favor the formation of new heterocyclic compounds by attack of nucleophilic part of the dipolar reagent on the C-8 site of C8=N2 bond.

**Table 10**

Non-linear optical property

Nonlinear optics deals with the interaction of applied electromagnetic fields in various materials to generate new electromagnetic fields, altered in wave number, phase, or other physical properties [73]. Organic molecules able to manipulate photonic signals efficiently are of importance in technologies such as optical communication, optical computing, and dynamic image processing [74]. DFT has been extensively used as an effective method to investigate NLO properties of organic materials. In order to gain insight into NLO property of title compound, the first static hyperpolarizability ( $\beta$ ) were calculated by the finite field perturbation method in vacuum as well as incorporating the solvent factors with increasing polarity. First hyperpolarizability is a third rank tensor that can be described by a  $3 \times 3 \times 3$  matrix. The 27 components of the 3D-matrix can be reduced to 10 components due to the Kleinman symmetry [75]. The components of  $\beta$  are defined as the coefficients in the Taylor series expansion of the energy in the external electric field. When the external electric field is weak and homogeneous this expansion becomes:

$$E = E^0 - \mu_i F_i - 1/2\alpha_{ij} F_i F_j - 1/6\beta_{ijk} F_i F_j F_k + 1/24\gamma_{ijkl}$$

Where  $E^0$  is the energy of the unperturbed molecules,  $F_i$  the field at the origin and  $\mu_i$ ,  $\alpha_{ij}$  and  $\beta_{ijk}$  are the components of dipole moment, polarizability, and the first hyperpolarizability respectively. Using the x, y and z components of  $\beta$  obtained from Gaussian 09 output, the magnitude of the mean first hyperpolarizability tensor can be calculated.

The calculated first hyperpolarizability ( $\beta_0$ ) of the title compound in vacuum is  $8.36 \times 10^{-30}$  esu, which is comparable with the reported values of related compounds [76]. The  $\beta_0$  value is about 10 times more than the  $\beta_0$  magnitude of standard p-nitro aniline ( $\beta_0 = 0.83 \times 10^{-30}$  esu) and 66.38 times than that of standard NLO material urea ( $0.13 \times 10^{-30}$  esu). The  $\beta_0$  value was found to increase slightly with polarity of solvent (Table 11). The calculated results show much better first order non-linear optical (NLO) response. We conclude that the title compound is an attractive object for future studies of nonlinear optical properties.

**Table 11**

Quantum theory of atoms in molecules (QTAIMs) analysis

Molecular graph of the compound **3**, using AIM program at B3LYP/6-31G (d, p) level is shown in Fig. 11. Geometrical as well as topological parameters are given in Supplementary material (S Table 2). The various type of interactions visualized in molecular graph are classified on the basis of geometrical, topological and energetic parameters (discussed as Supplementary material). In this article, the *Bader's theory* application is used to estimate hydrogen bond energy (E). Espinosa [77] proposed proportionality between hydrogen bond energy (E) and potential energy density ( $V_{BCP}$ ) at H—O contact:  $E = 1/2(V_{BCP})$ . Weak intramolecular hydrogen bond was found to be present between N2 ... H34 and O17...H31. According to AIM calculations, the total intramolecular H-bond energy was calculated as -12.44 kcal/mol. The ellipticity ( $\epsilon$ ) at BCP is a sensitive index to monitor the  $\pi$ -character of

bond. The  $\varepsilon$  is related to  $\lambda_1$  and  $\lambda_2$ , which correspond to the eigen values of Hessian and defined by relationship:  $\varepsilon = (\lambda_1/\lambda_2) - 1$ . The ellipticities ( $\varepsilon$ ) of bond of aromatic rings at BCP are in range of 0.176-0.310. The lower values of ellipticity ( $\varepsilon$ ) confirm that there is delocalization of electron in aromatic rings. The ellipticity of chain C=C and N=N (in range 0.267-0.310), suggests that these bonds extends conjugation through delocalization of aromatic ring electrons. The overall ellipticity value suggests that there is strong delocalization in the molecule.

**Fig 11**

#### Statistical thermodynamics

On the basis of vibrational analysis and statistical thermodynamics, the standard thermodynamics functions: heat capacity  $C_{p,m}^0$ , entropy  $S_m^0$  and enthalpy  $H_m^0$  were obtained at B3LYP/6-31G (d, p) and are listed in Table 12. It is found that the standard heat capacities, entropies and enthalpy changes are increasing with temperatures ranging from 100 to 600 K due to the fact the molecular vibrational intensities are increasing with temperatures. The correlation equations between heat capacities, entropies, enthalpy changes and temperatures were fitted by quadratic formula. Correlation graphs of thermodynamic functions vs. temperature (T) are shown in Supplementary materials (S Figs. 8, 9 and 10). The corresponding fitting equations between thermodynamic properties and temperature are as follows:

$$H_m^0 = 211.7 + 0.019T + 0.000T^2, (R^2 = 0.999)$$

$$C_{p,m}^0 = 15.78 + 0.349T - 0.000T^2 (R^2 = 0.999)$$

$$S_m^0 = 74.09 + 0.412T - 0.000T^2 (R^2 = 0.999)$$

These equations above can be used to compute other thermodynamic functions and can estimate the directions of chemical reactions according to the second law of thermodynamics

in thermo-chemical field [78]. These equations will be helpful for the further studies of the title compound.

### Table 12

#### Conclusion

The structure of the titled compound was confirmed by IR,  $^1\text{H}$  NMR,  $^{13}\text{C}$  NMR and single crystal X-ray diffraction. The geometrical parameters of the title compound are in agreement with the XRD results.  $^1\text{H}$  and  $^{13}\text{C}$  NMR chemical shift were calculated with the help of gauge-including atomic orbital (GIAO) approach showing good agreement with experimental chemical shift. The vibrational wave numbers were examined theoretically and the normal modes were assigned by potential energy distribution calculation. The UV-Visible spectrum of compound studied by TD-DFT shows strong  $\pi \rightarrow \pi^*$  transitions. The calculated HOMO-LUMO band gap shows the chemical reactivity and supports bioactivity of the molecule. A computation of the first hyperpolarizability ( $\beta_0$ ) indicates that compound may be a good candidate as a NLO material. Using NBO analysis the stability of the molecule arising from hyper-conjugative interaction and charge delocalization through  $\pi$ -conjugated bridge has been analyzed. Intra-molecular hydrogen interaction and ellipticity studied by AIM approach showed weak hydrogen interactions and  $\pi$ -character of bond in aromatic ring. The calculated maximum local electrophilic reactivity descriptors for C-8, indicates the favorable site for nucleophilic attack at this position and favors the formation of new heterocyclic compounds.

#### Acknowledgement

The authors are thankful to the UGC major research project (F.No.39-701/2010-SR) and SAIF- CDRI, Lucknow for providing spectral measurements facilities. We are thankful to our department for providing center facility for computational research and chemistry department

of BHU, Varanasi for single crystal X-ray diffraction. Authors would also like to thank Abhinav Kumar of our department for solving crystal structure.

### Supplementary materials

CCDC **1018654** contains the supplementary crystallographic data for the title compound. These data can be obtained free of charge at, <http://www.ccdc.cam.ac.uk/conts/retrieving.html>, or from Cambridge Crystallographic data Center, 12 Union Road, Cambridge CB21EZ, UK; fax (+44) 1223 336 033; or email:deposit@ccdc.cam.ac.uk. Supplementary data associated with this article can be found, in the online version of this article.

### References

- [1] X. Deng, N.S. Mani, *Org. Lett.* 10 (2008) 1307.
- [2] X. Deng, N.S. Mani, *J. Org. Chem.* 73 (2008) 2412.
- [3] Y. Nakayama, Y. Sanemitsu, *J. Org. Chem.* 49 (1984) 1703.
- [4] H. N. Dogan, A. Duran, S. Rollas, G. Sener, Y. Armutak, M. K. Uysal, *Med. Sci. Res.* 26 (1998) 755.
- [5] S. G. Küçükgülzel, A. Kocatepe, E. De Clercq, F. Sahin, *Eur. J. Med. Chem.* 41 (2006) 353.
- [6] S. G. Küçükgülzel, E. E. Oruç, S. Rollas, F. Sahin, A. Ozbek, *Eur. J. Med. Chem.* 37 (2002) 197.
- [7] V. N. Korotchenko, A. V. Shastin, V. G. Nenaidenko, E. S. Balenkova, *Russ. J. Org. Chem.* 39 (2003) 527.
- [8] V. O. Kozminykh, A. O. Belyaev, Bukanova, E.V. Kozminykh, T.F. Odegova, *J.Pharm. Chem.* 38 (2004) 368.
- [9] L. W. Zheng, L. L. Wu, B. X. Zhao, W. L. Dong, J. Y. Miao, *Bioorg. Med. Chem.* 17 (2009) 1957.
- [10] D. Sriram, P. Yogeeswari, R.V. Devakaram, *Bioorg. Med. Chem.* 14 (2006) 3113.
- [11] M. Yu, H. Lin, *Ind. J. Chem. Sec. A* 46 (2007) 1437.
- [12] T. L. Smalley, A. J. Peat Jr., J. A. Boucheron, S. Dickerson, D. Garrido, F. Preugschat, S. L. Schweiker, S.A. Thomson, T. Y. Wang, *Bioorg. Med. Chem.* 16 (2006) 2091.
- [13] N. Raman, S. Ravichandran, C. Thangaraja, *J. Chem. Sci.* 116 (2004) 215.
- [14] J. P. Jasinski, C. J. Guild, C. S. C. Kumar, H. S. Yathirajan, A. N. Mayekar, *Bull. Korean Chem. Soc.* 31(2010) 881.
- [15] L. Lilib, L. A. Mohamed, M. F. Iskander, *Transition Met. Chem.* 25 (2002) 700.
- [16] M. A. Affan, I. P. P. Foo, B. A. Fasihuddin, E. U. H. Sim, M.A. Hapipah, *J. Anal. Sci.* 13(2009) 73.
- [17] M. Yu, H. Lin, H. Lin, *Ind. J. Chem. Sec. A* 46 (2007) 1437.

- [18] B. Szczesna, U. Lipkowska, *Supramol. Chem.* 13 (2001) 247.
- [19] S. Vijayakumar, A. Adithya, K. N. Sharafudeen, B. K. Chandrasekharan, *J. Mod. Optic* 57 (2010) 670.
- [20] C. H. Chen, J. M. Shi, *Coord. Chem. Rev.* 171(1998)161.
- [21] M. M. Bader, T. Hamada, A. Kakutta, *J. Am. Soc.* 114 (1992) 6475.
- [22] A.K. Singh, G. Saxena, R. Prasad, A .Kumar, *J. Mol. Struct.* 1017 (2012) 27.
- [23] L.J. Furrugia, *J. Appl. Cryst.* 32(1999) 837-838.
- [24] SHEL X 97, G.M. Sheldrick, *Acta Cryst.* (2008) 112-122.
- [25] M.N. Burnett, C. K. Jhonson, ORTEP. III Oak Ridge Thermal Ellipsoid plot, Program for Crystal structure Illustration, Report ORNL-6895, Oak Ridge National Laboratory, Oak Ridge, TN, USA, 1996.
- [26] Frisch et al., *Gaussian 09 Revision B.01*, Gaussian, Inc., Wallingford, CT, 2010.
- [27] K. Wolinski, J. F. Hinton, P. Pulay, *J. Am. Chem. Soc.* 112 (1990) 8251–8260.
- [28] T. Yanai, D. P. Tew, N. C. Handy, *Chem. Phys Let.* 393 (2004) 51-57.
- [29] J. Preat, *J Phys Chem. Comm.* 114 (2010)16716-16725.
- [30] B. Camino, M. De-La-Pierre, A. M. Ferrari, *J. Mol. Struct.* 1046 (2013) 116–123.
- [31] A. Irfan, R. Jin, A. G. Al-Sehemi, A. M. Asiri, *Spectrochim Acta Part A: Mol. Biom. Spectr.* 110 (2013) 60-66.
- [32] V. Barone, M. Cossi, J. Thomasi, *J.Comput.Chem.*19 (1998) 404-417.
- [33] M. Sarafran, A. Komasa, E. B. Adamska, *J. Mol. Struct.* 827 (2007) 101-107.
- [34] J. M. L. Martin, V. Alsenoy, C. V. Alsenoy, *Gar2ped*, University of Antwerp, 1995.
- [35] P. Pulay, G. Fogarasi, F. Pang, J. E. Boggs, *J. Am. Chem. Soc.* 101 (1979) 2550.
- [36] *Computer program Gauss View 5.0.9*, Gaussian Inc, Wallingford, CT 06492 USA.
- [37] R. F. W. Bader, *Atoms in Molecules, A Quantum Theory*, Oxford University Press, Oxford, 1990.
- [38] A. Ozdemir, G. Turan–Zitoumi, Z. A. Kaplancikli, M. D. Altinop, *J. Serb. Chem. Soc.* 77(2) (2012) 141–146.
- [39] R. M. Silverstein, F.X. Webster, *Spectrometric Identification of Organic Compounds*, sixth ed., John Wiley, Asia, 2012.
- [40] R. M. Silverstein, F.X. Webster, *Spectrometric Identification of Organic Compounds*, sixth ed., John Wiley, Asia, 2003.
- [41] G. Smith, D. E. Lynch, K. A. Byriell, C. H. L. Kennard, *Aust. J. Chem.* 48 (1995) 1133–1149.
- [42] R. D. Chambers, M. A. Fox, G. Sandford, J. Trmcic, A. Goeta, *J. Fluorine Chem.* 128 (2007) 29–33.
- [43] N. Sundaraganesan, S. Ayyappan, H. Umamaheswari, B.D. Joshua, *Spectrochim. Acta* 66A (2007) 17–27.
- [44] A. Saeed, S. Hussain, U. Florke, *Turk. J. Chem.* 32 (2008) 481–486.

- [45] Y. S. Mary, H. T. Varghese, C. Y. Panicker, T. Ertan, I. Yildiz, O. Temiz-Arpaci, *Spectrochim. Acta* 71A (2008) 566–571.
- [46] R. Minitha, Y. S. Mary, H. T. Varghese, C. Y. Panicker, R. Ravindran, K. Raju, V. M. Nair, *J. Mol. Struct.* 985 (2011) 316–322.
- [47] J. C. Espinoza-Hicks, L. M. Rodriguez-Valdez, G. V. Nevarez-Moorillon, A. Camacho-Davila, *J. Mol. Struct.* 1020 (2012) 88–95.
- [48] J. A. Pople, H. B. Schlegel, R. Krishnan, D. J. Defrees, J. S. Binkley, M. J. Frisch, R. A. Whiteside, R.F. Hout, W. J. Hehre, *Int. J. Quantum Chem.* 15 (1981) 269–278.
- [49] L. J. Bellamy, *The Infrared Spectrum of Complex Molecules*, third ed. Chapman and Hall, London, 1975.
- [50] M. Barthes, G. De Nunzio, G. Ribet, *Synth Met.* 76 (1996) 337–340.
- [51] R. M. Silverstein, F.X. Webster, *Spectrometric Identification of Organic Compounds*, sixth ed., John Wiley, Asia, 2003.
- [52] A. Perjessy, D. Rasala, P. Tomasik, R. Gawinecki, *Collect. Czech. Chem. Commun.* 50 (1985) 2443–2452.
- [53] J. F. Brown Jr., *J. Am. Chem. Soc.* 77 (1955) 6341–6351.
- [54] N. P. G. Roeges, *A Guide to the Complete Interpretation of Infrared Spectra of Organic Structures*, Wiley, New York, 1994.
- [55] G. Varsanyi, E. Molner-Pall, K. Kosa, G. Keresztury, *Acta Chim. Acad. Sci. Hung.* 106 (1979) 481–498.
- [56] V. Suryanarayana, A. P. Kumar, G. R. Rao, G. C. Panday, *Spectrochim. Acta* 48A (1992) 1481–1489.
- [57] P. Pulay, G. Fogarasi, F. Pang, J. E. Boggs, *J. Am. Chem. Soc.* 101 (1979) 2550–2560.
- [58] J. Coates, in: R. A. Meyers (Ed.), *Encyclopedia of Analytical Chemistry; Interpretation of Infrared Spectra, A practical Approach*, John Wiley and Sons Ltd. Chichester, 2000.
- [59] K. Wolinski, J. F. Hinton, J. F. Pulay, *J. Am. Chem. Soc.* 112 (1990) 8251–8260.
- [60] J. Fleming, *Frontier Orbitals and Organic Chemical Reactions*, 249 s, Wiley, London, 1976.
- [61] S. W. Xia, X. Xu, Y. L. Sun, Y. L. Fan, Y. H. Fan, C. F. Bi, D. M. Zhang, L. R. Yang, *Chin. J. Struct. Chem.* 25 (2006) 849.
- [62] E. Scrocco, J. Tomasi, *Adv. Quantum. Chem.* 11 (1978) 115–193.
- [63] F. J. Luque, J. M. Lopez, M. Orozco, *Theor. Chem. Acc.* 103 (2000) 343–345.
- [64] E. Scrocco, J. Tomasi, *Curr. Chem.* 7 (1973) 95–170.
- [65] I. M. Snehalatha, C. Ravikumar, I. Joe Hubert, N. Sekar, V. S. Jayakumar, *Spectrochim. Acta Part A: Mol. Biomol. Spectrosc.* 72 (2009) 654–662.
- [66] D. Geo, L. Goodman, *J. Phys. Chem.* 100 (1996) 125400–12545.
- [67] C. G. Liu, Z. M. Su, X. H. Guan, S. Muhammad, *J. Phys. Chem. C* 115 (2011) 23946–23954.
- [68] J. Padmanabhan, R. Parthasarathi, V. Subramanian, P. K. Chattaraj, *J. Phys. Chem. A* 111 (2007) 1358.

- [69] R. G. Parr, W. Yang, Density Functional Theory of Atoms and Molecules, Oxford University Press, Oxford, New York, 1989.
- [70] R. G. Parr, L. V. Szentpály, S. Liu, J. Am. Chem. Soc. 121 (1999) 1922.
- [71] R. G. Pearson, J. Org. Chem. 54 (1989) 1430–1432.
- [72] P. K. Chattaraj, S. Giri, S. Duley, Chem. Rev. 111 (2011) PR43-PR75.
- [73] Y. R. Shen, The Principles of Nonlinear Optics, Wiley, New York, 1984.
- [74] P.V. Kolinsky, Opt. Eng. 31 (1992) 11676-11684.
- [75] D. A. Kleinmann, Phys. Rev. 126 (1962) 1977.
- [76] L. N. Kuleshova, M. Y. Antipin, V. N. Khrustalev, D.V. Gusev, E. S. Bobriková, Kristallografiya 48 (2003) 594–601.
- [77] E. Espinosa, E. Molins, C. Lecomte, Chem. Phys. Lett. 285 (1998) 170.
- [78] W. Li X, E. Shibata, T. Nakamura, Mater. Transact. 44(5) (2003) 1004.

#### FIGURE CAPTION

**Fig.1.** Scheme with synthetic route for preparation of hydrazone compound.

**Fig.2.** ORTEP diagram of molecule at 30% probability with atom numbering scheme, hydrogen atoms are omitted for clarity.

**Fig.3.** Optimized geometry of compound **3** using B3LYP/6-31G (d, p) level of theory.

**Fig.4.** Calculated IR spectrum of compound **3**.

**Fig.5.** Correlation graph between experimental and calculated wave numbers of compound **3**.

**Fig.6.** Correlation graph between experimental and calculated  $^1\text{H}$  NMR chemical shifts of compound **3**.

**Fig.7.** Correlation graph between experimental and calculated  $^{13}\text{C}$  NMR chemical shifts of compound **3**.

**Fig.8.** UV-Visible spectrum of compound **3** in dichloromethane and ethanol.

**Fig.9.** Selected orbital transitions with their excitation energies (eV) obtained from TD-DFT/CAM-B3LYP calculation using PCM model for compound **3** in solvent dichloromethane.

**Fig.10.** Molecular electrostatic potential surface (MEP) of the compound **3** at B3LYP/6-31G (d, p) level of theory. (For interpretation of the references to color in this figure legend, the reader is referred to the web version of this article.).

**Fig.11.** Molecular graph of compound **3** at B3LYP/6-31G (d, p) level using AIM program: bond critical points (small green spheres), ring critical points (small black sphere), bond paths (dark grey lines). (For interpretation of the references to color in this figure legend, the reader is referred to the web version of this article.).

#### TABLE CAPTION

**Table 1** Crystal data and structure refinement.

**Table 2** Hydrogen-bond geometry for crystal structure.

**Table 3** Calculated enthalpy (au.), Gibbs free energy (au.), entropy (cal/mol K) for **1**, **2**, **3**, **4** and reaction.

**Table 4** Comparison of selected optimized geometrical parameters of compound **3** with experimental XRD parameters.

**Table 5** Experimental and calculated vibrational wave numbers ( $\text{cm}^{-1}$ ) of **3** at B3LYP/6-31G (d, p) level and their assignments.

**Table 6** Comparison between calculated and experimental  $^1\text{H}$  and  $^{13}\text{C}$  NMR chemical shifts  $\delta$  (ppm) for compound **3** in  $\text{CDCl}_3$  as the solvent at (25°C).

**Table 7** Selected TD-DFT excitations and approximate assignments for compound **3**.

**Table 8** Second order perturbation theory analysis of Fock matrix in NBO basis for selected donor (Lewis) and acceptor (non-Lewis) orbitals.

**Table 9**

Calculated  $E_{\text{HOMO}}$ ,  $E_{\text{LUMO}}$ , energy band gap ( $E_{\text{L}} - E_{\text{H}}$ ), chemical potential ( $\mu$ ), electronegativity ( $\chi$ ), global hardness ( $\eta$ ), global softness ( $S$ ) and global electrophilicity index ( $\omega$ ) (in eV) for reactants **1**, **2**, product **3** at B3LYP/6-31G (d, p) level.

**Table 10**

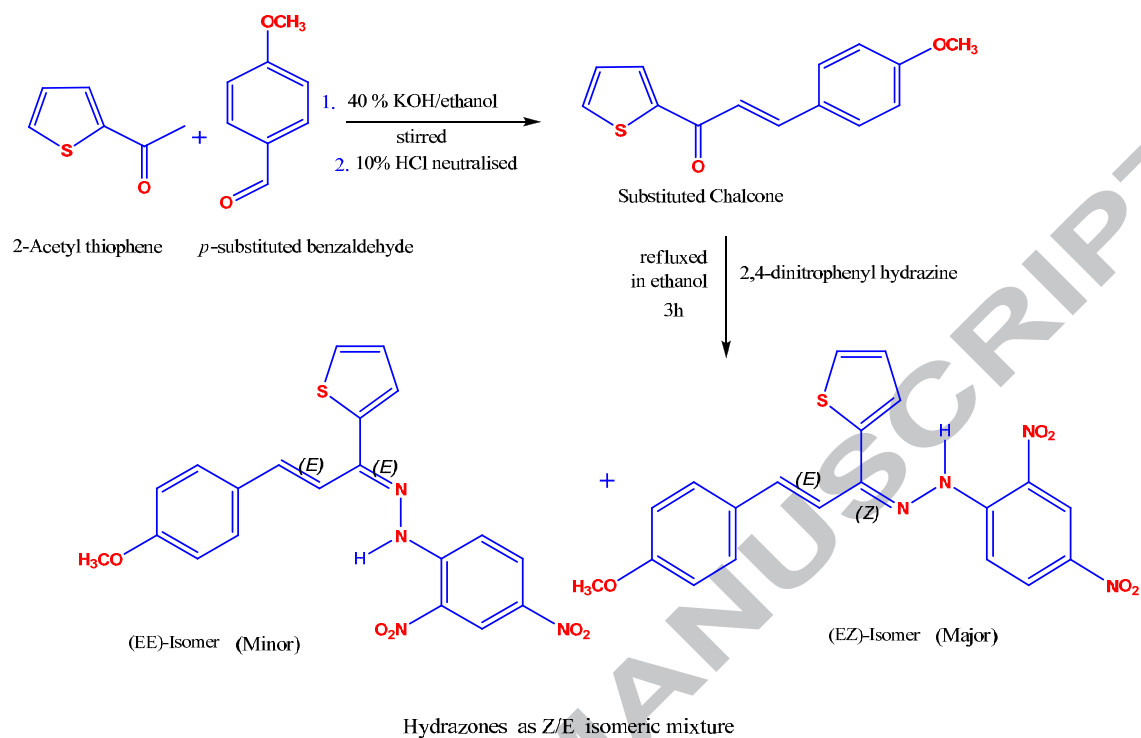
Selected electrophilic reactivity descriptors ( $f_k^+$ ,  $s_k^+$ ,  $\omega_k^+$ ) and nucleophilic reactivity descriptors ( $f_k^-$ ,  $s_k^-$ ,  $\omega_k^-$ ) of reactants **1**, **2** and product **3** using Hirshfeld atomic charges.

**Table 11**

Dielectric constant ( $\epsilon$ ) for solvents, dipole moment ( $\mu_0$ ) (Debye), polarizability ( $\alpha_0$ ) ( $10^{-24}$  esu), anisotropy of polarizability ( $\Delta\alpha$ ) ( $10^{-24}$  esu) and calculated first static hyperpolarizability ( $\beta_0$ ) ( $10^{-30}$  esu) for compound **3**.

**Table 12.** Thermodynamic properties of compound **3** at different temperatures.

## Figures



## Scheme

Fig. 1. Scheme with synthetic route for preparation of hydrazone compound.

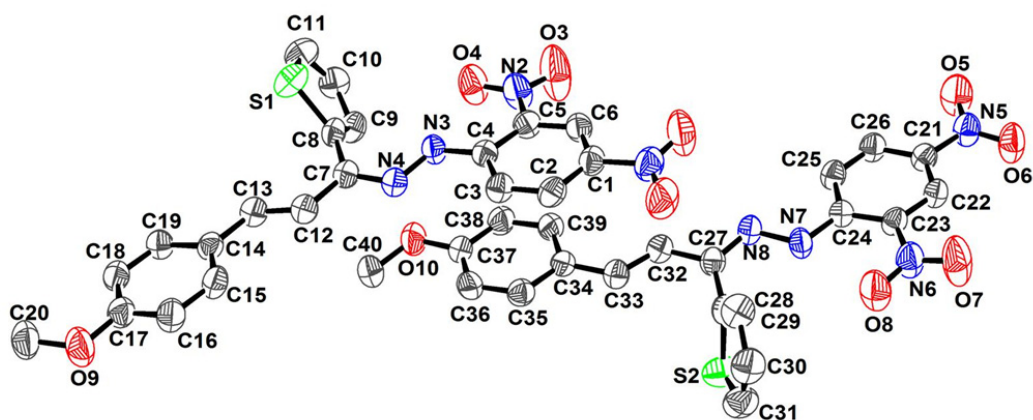


Fig. 2. ORTEP diagram of molecule at 30% probability with atom numbering scheme, hydrogen atoms are omitted for clarity.

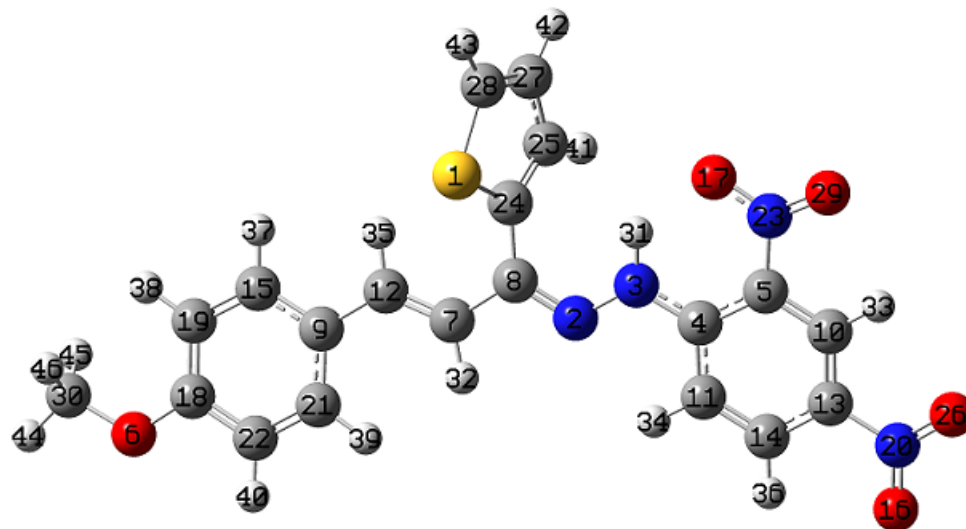


Fig. 3. Optimized geometry of compound 3 using B3LYP/6-31G (d, p) level of theory.

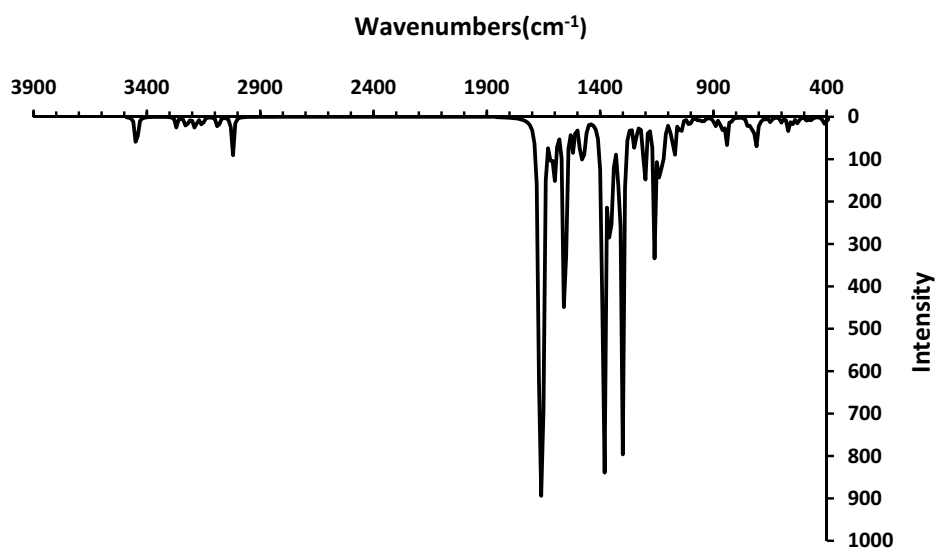


Fig. 4. Calculated IR spectrum of compound 3.

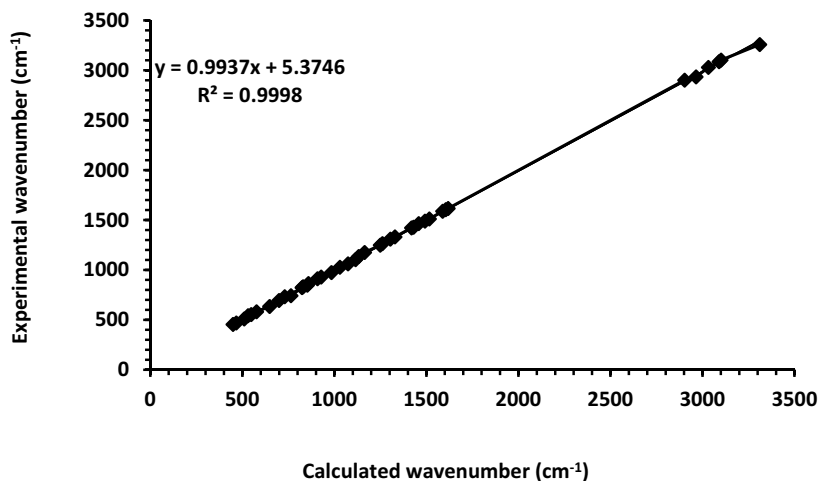


Fig. 5. Correlation graph between experimental and calculated wave numbers of compound 3.

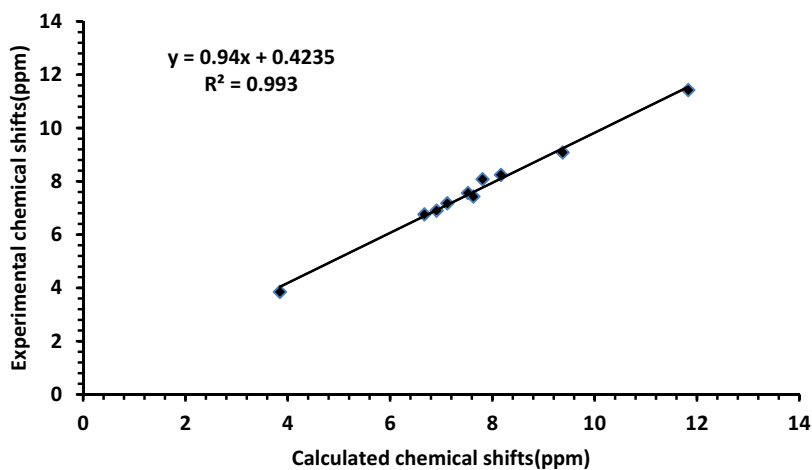
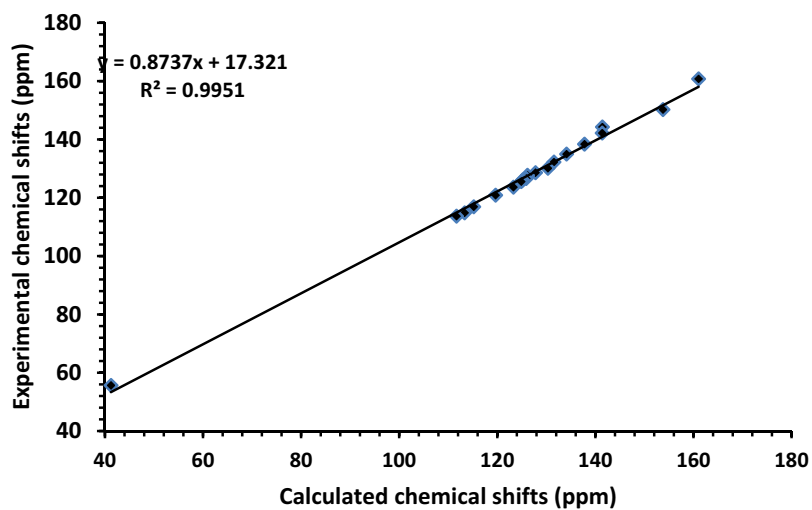
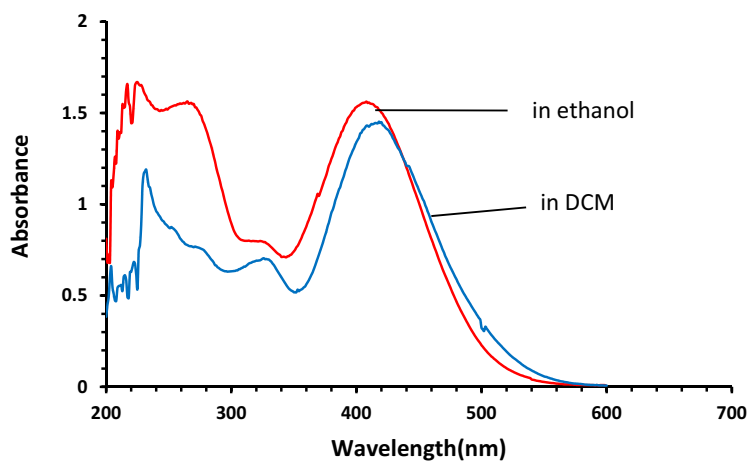


Fig. 6. Correlation graph between experimental and calculated <sup>1</sup>H NMR chemical shifts of compound 3.



**Fig. 7.** Correlation graph between experimental and calculated <sup>13</sup>C NMR chemical shifts of compound 3.



**Fig. 8.** UV-Vis. spectrum of compound 3 in dichloromethane and ethanol.

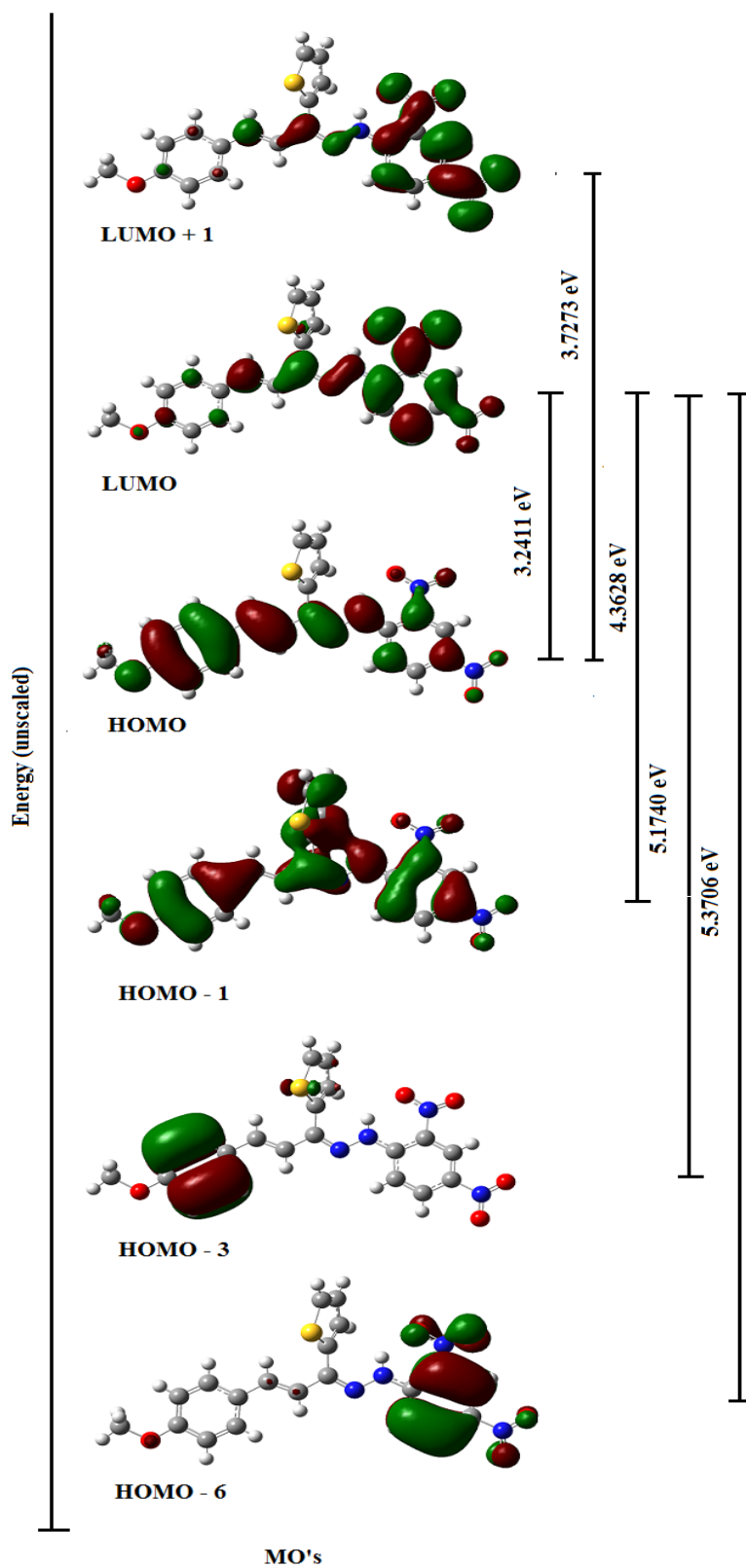


**Fig.9.** Selected orbital transitions with their excitation energies (eV) obtained from TD-DFT/CAM-B3LYP calculation using PCM model for compound **3** in solvent dichloromethane.

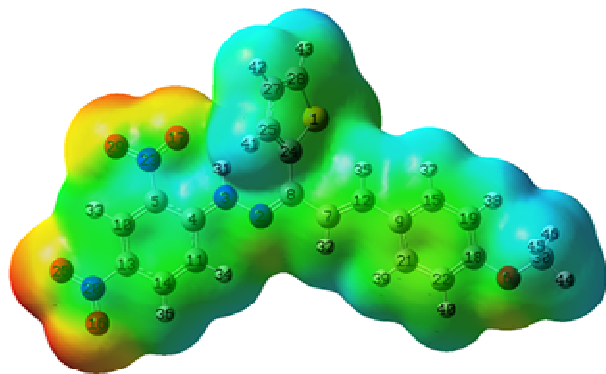


**Fig. 10.** Molecular electrostatic potential surface (MEP) of the compound **3** at B3LYP/6-31G (d, p) level of theory. (For interpretation of the references to colour in this figure legend, the reader is referred to the web version of this article).

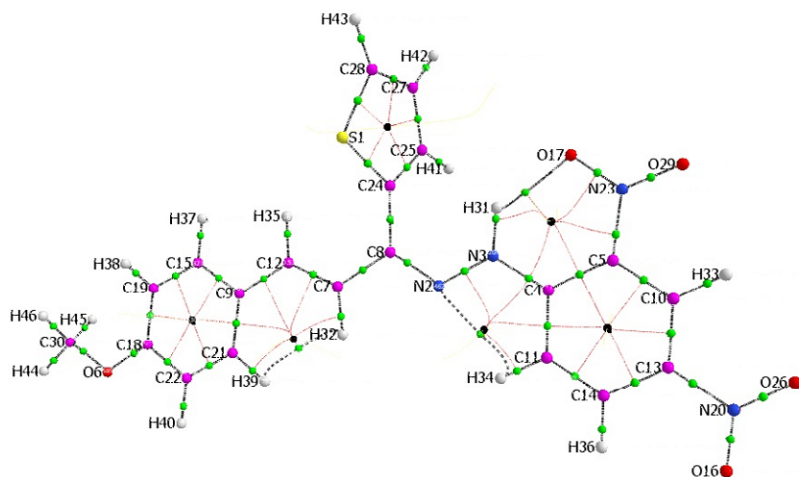


**Fig. 11.** Molecular graph of compound **3** at B3LYP/6-31G (d, p) level using AIM program: bond critical points (small green spheres), ring critical points (small black sphere), bond paths (dark grey lines). (For interpretation of the references to color in this figure legend, the reader is referred to the web version of this article.)

CCDC deposition number	<b>1018654</b>
Empirical formula	C <sub>20</sub> H <sub>16</sub> N <sub>4</sub> O <sub>5</sub> S
Formula weight	423.43
Color and habit	Reddish brown, plate
Crystal size( mm)	0.300 x 0.220 x 0.200
Crystal system, Space group	Triclinic, P -1
a ( Å)	8.6760(10)
b ( Å)	11.9620(10)
c ( Å)	19.622(2)
a (°)	94.358(7)
b (°)	99.105(7)
g (°)	95.689(6)
V ( Å <sup>3</sup> )	1950.9(2)
Z, D <sub>c</sub> (mg/m <sup>3</sup> )	4, 1.412
μ(mm <sup>-1</sup> )	0.203
T(K)	298(2)
λ(Mo Ka) ( Å)	0.71073
Theta range for data collection(°)	3.062 to 29.189
Refinement method	Full-matrix least-squares
Max. and min. transmission	0.960 and 0.942
Largest diff. peak and hole( e. Å <sup>-3</sup> )	0.462 and -0.294
Completeness to theta	99.8 %(25.24°)
F(000)	876
No. of reflection(Unique)	16081/9030
No. of refined parameters	541
Data / restraints / parameters	9030 / 0 / 541
R factor [I > σ(I)]	0.0667
wR2[I > σ(I)]	0.1590
R factor (all data)	0.1610
wR2 (all data)	0.2232
GooF (S)	1.013

**Table 1**  
Crystal data and structure refinement.

**Table 2**

Hydrogen-bond geometry for crystal structure.

D-H...A	D-H(Å)	H...A(Å)	D...A(Å)	D-H...A(°)
N3-H1A...O4	0.88	1.99	2.6095(3)	126
N3-H1A...N2	0.88	2.62	2.9019(3)	100
N7-H2A...O8	0.85	1.98	2.6050(3)	130
N7-H2A...N6	0.85	2.61	2.9127(3)	103
C2-H2...O9	0.93	2.67	3.5891(4)	169
C3-H3...N4	0.93	2.47	2.7864(3)	100
C9-H9...O10	0.93	2.49	3.3301(4)	150
C19-H19...O7 <sup>(a)</sup>	0.93	2.59	3.4573(4)	155
C20-H20A...O1 <sup>(b)</sup>	0.96	2.49	3.2795(4)	140
C25-H25...N8	0.93	2.46	2.7769(3)	100
C29-H29...O1 <sup>(c)</sup>	0.93	2.60	3.5569(4)	139
C38-H38...O5 <sup>(d)</sup>	0.93	2.49	3.3434(4)	152

**Symmetry codes:** (a) -1+x, y, -1+z (b) 2-x, -y, -z (c) 2-x, -y, 1-z (d) 1-x, 1-y, 1-z

**Table 3**

Calculated enthalpy (au.), Gibbs free energy (au.), entropy (cal/mol K) for **1**, **2**, **3**, **4** and reaction.

Thermodynamic parameters	1	2	3	4	Reaction <sup>a</sup>
Enthalpy (H)	-1089.0983	-751.7867	-1764.4885	-76.395	0.0019
Gibbs free energy (G)	-1089.1597	-751.8385	-1764.5774	-76.416	0.0048
Entropy (S)	129.128	108.994	187.102	45.116	-5.90

<sup>a</sup> Reaction: **1**+**2** (reactants) → **3**+**4** (products); **1** = (E)-3-(4-methoxyphenyl)-1-(thiophen-2-yl)prop-2-en-1-one; **2** = 2, 4-dinitrophenyl hydrazine; **3** = (Z)-1-(2, 4-dinitrophenyl)-2-((E)-3-(4-methoxyphenyl)-1-(thiophen-2-yl)allylidene) hydrazine; **4** = H<sub>2</sub>O

**Table 4**

Comparison of selected optimized geometrical parameters of compound **3** with experimental XRD parameters.

Bond length(Å)	Bond angle(°)		Dihedral angle(°)	
	Calcd	Exp.	Calcd	Exp.

S1-C24	1.75	1.73(3)	C24-S1-C28	91.7	91.9(2)	C28-S1-C24-C8	178.0	177.6(3)
S1-C28	1.73	1.69(4)	N3-N2-C8	118.5	116.9(3)	C8-N2-N3-C4	178.9	176.1(3)
N2-N3	1.35	1.39(4)	N2-N3-C4	120.3	120.8(2)	C8-N2-N3-H31	0.64	-8.6(2)
N2-C8	1.31	1.30(4)	N2-N3-H31	122.5	117.0(2)	N3-N2-C8-C7	-178.1	-179.4(3)
N3-C4	1.36	1.35(4)	C4-N3-H31	117.3	122.0(2)	N3-N2-C8-C24	1.2	-0.6(4)
N3-H31	1.02	0.88(3)	N3-C4-C5	122.7	122.6(3)	N2-N3-C4-C5	-179.2	174.5(3)
C5-N23	1.45	1.44(5)	N3-C4-C11	120.3	121.5(3)	N2-N3-C4-C11	0.9	-5.2(4)
O6-C18	1.36	1.36(5)	C8-C7-C12	125.4	126.1(3)	H31-N3-C4-C5	-0.9	-0.6(2)
O6-C30	1.42	1.43(4)	N2-C8-C7	115.2	115.4(3)	H31-N3-C4-C11	178.6	179.6(2)
C7-C8	1.45	1.45(5)	N2-C8-C24	123.4	123.0(3)	C30-O6-C18-C22	179.6	170.7(3)
C7-C12	1.35	1.33(5)	C7-C8-C24	121.5	121.6(3)	C30-O6-C18-C19	-0.24	-8.3(5)
C8-C24	1.48	1.48(5)	C12-C9-C15	118.9	119.6(3)	C12-C7-C8-N2	-173.3	172.9(3)
C7-H32	1.09	0.93(3)	C12-C9-C21	123.8	124.0(3)	C12-C7-C8-C24	7.03	8.4(4)
C12-H35	1.09	0.93(4)	C7-C12-C9	127.1	127.0(3)	H32-C7-C8-C24	-174.4	-171.7(3)
C13-N20	1.46	1.46(4)	S1-C24-C8	121.4	121.2(2)	N2-C8-C24-S1	-115.5	-116.8(3)
C9-C12	1.46	1.45(5)	C8-C24-C25	128.2	128.6(3)	N2-C8-C24-C25	62.0	61.1(5)
C24-C25	1.38	1.36(5)	O29-N23-O17	122.8	121.7(4)	C7-C8-C24-S1	64.2	61.4(4)
C25-C27	1.43	1.40(5)	O26-N20-O16	124.7	123.1(4)	C7-C8-C24-C25	-118.3	-120.3(4)
C27-C28	1.38	1.35(5)	C18-O6-C30	118.4	117.9(3)	C15-C9-C12-C7	-177.8	178.5(3)
C4-C5	1.43	1.42(5)	C25-C27-C28	112.6	112.5(3)	C21-C9-C12-C7	2.3	2.6(6)
C5-C10	1.39	1.37(5)	C24-C25-C27	113.5	113.2(3)	C8-C7-C12-C9	-179.8	-178.6(3)
C4-C11	1.42	1.41(4)	S1-C24-C25	110.3	110.2(3)	H32-C7-C12-H35	-178.1	-178.6(3)
C11-C14	1.38	1.35(5)	S1-C28-C27	111.9	112.2(3)			
C13-C14	1.41	1.40(5)	C5-C4-C11	117.1	116.0(3)			
C10-C13	1.38	1.36(5)	C10-C13-C14	121.0	121.5(3)			
C9-C15	1.41	1.39(5)	C4-C5-C10	121.1	121.9(3)			
C9-C21	1.41	1.41(5)	C4-C11-C14	121.5	122.4(3)			
C21-C22	1.38	1.38(5)	C9-C21-C22	121.3	121.1(3)			
C18-C22	1.41	1.38(5)	C9-C15-C19	122.2	122.9(3)			
C18-C19	1.39	1.38(5)	C15-C9-C21	117.3	116.3(3)			
C15-C19	1.39	1.37(5)	C18-C22-C21	120.4	120.7(3)			

**Table 5**Experimental and calculated vibrational wave numbers ( $\text{cm}^{-1}$ ) of **3** at B3LYP/6-31G (d, p) level and their assignments.

modes	Calculated		Obs.	IR <sub>int</sub>	Vibrational assignments (PED $\geq$ 10%)
	Unscaled	Scaled			
132.	3446	3311	3258	102.88	$\nu(\text{N3H31})(99)$
131.	3270	3142	-	23.82	$\nu(\text{C10H33})(99)$
130.	3267	3139	-	0.66	$\nu(\text{C28H43})(92)$
129.	3259	3131	-	0.65	$\nu(\text{C11H34})(87)\nu(\text{C14H36})(12)$

128.	3243	3116	-	1.92	v(C14H36)(87)-v(C11H34)(12)
127.	3235	3108	-	2.16	v(C27H42)(71)v(C25H41)(22)
126.	3227	3101	3102	20.88	v(C19H38)(96)
125.	3219	3093	-	2.85	v(C25H41)(76)-v(C27H42)(22)
124.	3216	3090	3086	8.92	v(C22H40)(77)v(C21H39)(22)
123.	3199	3074	-	2.89	v(C21H39)(60)-v(C22H40)(20)v(C7H32)(18)
122.	3189	3064	-	20.36	v(C7H32)(74)-v(C21H39)(15)
121.	3182	3057	-	10.08	v(C15H37)(88)
120.	3174	3050	-	2.39	v(C12H35)(81)
119.	3156	3032	3029	28.02	v(C30H44)(90)
118.	3086	2965	2934	37.37	v(C30H45)(50)-v(C30H46)(50)
117.	3021	2903	2901	96.34	v(C30H46)(46)v(C30H45)(45)
116.	1684	1618	1616	16.92	v(C7C12)(45)-(δ-C7C8H32)(11)
115.	1670	1605	1604	426.82	v(C11C14)(17)v(C5C10)(11)-v(C10C13)(10)
114.	1661	1596	-	604.11	v(C21C22)(15)v(C15C19)(10)
113.	1653	1588	1588	693.75	v(O16N20)(22)-v(N20O26)(20)
112.	1620	1556	-	20.62	v(N23O29)(27)-v(O17N23)(17)(δ-N2N3H31)(14)
111.	1614	1551	-	95.22	v(C18C19)(20)v(C9C20)(14)-v(C18C22)(12)-v(C9C15)(12)
110.	1599	1536	-	103.49	v(N2C8)(18)-v(N20O26)(13)v(O16N20)(12)-v(C10C13)(11)
109.	1596	1533	-	35.24	v(N2C8)(20)v(C24C25)(11)
108.	1578	1516	1511	4.12	v(N2C8)(27)-v(C24C25)(19)v(C27C28)(15)
107.	1559	1498	-	339.50	δ(C21H39)(11)δ(C15H37)(10)
106.	1553	1492	1489	334.83	v(N3C4)(23)v(C13C14)(17)
105.	1518	1458	1464	68.95	(δas-Me)(60)(δas-Me)(26)-(δ-C30O6H44)(10)
104.	1506	1447	-	6.52	(δas-Me)(65)-(δas-Me)(25)
103.	1489	1431	-	24.19	v(C27C28)(27)-(δs-Me)(20)v(C25C27)(14)-v(C24C25)(13)
102.	1488	1430	1428	26.42	(δs-Me)(58)v(C27C28)(11)
101.	1477	1419	1421	104.67	(δ-N2N3H31)(19)-v(C10C13)(14)-v(N23O29)(11)
100.	1470	1412	-	13.79	v(C21C22)(23)-v(C15C19)(21)-(C19H38)(11)
99.	1466	1409	-	37.50	v(C5C10)(30)-v(C11C14)(21)
96.	1383	1329	1331	886.54	v(O16N20)(20)v(N20O260)(16)-v(C13N20)(12)
95.	1378	1324	-	140.08	(δ-C12C9C7)(18)-v(C9C15)(12)
94.	1357	1304	1309	243.14	v(C4C5)(12)-v(O17N23)(12)-v(N23O29)(12)v(C10C13)(11)
93.	1352	1299	-	139.19	(δ-C12C9C7)(25)
92.	1337	1285	-	55.58	(δ-C9C12C7)(21)
91.	1321	1269	-	70.51	v(C7C8)(12)-(δ-C9C12C7)(11)
90.	1312	1261	1264	91.84	(δ-C7C8H32)(24)v(O6C18)(21)
89.	1300	1249	1248	769.10	v(O6C18)(19)-v(C15C19)(10)
88.	1292	1241	-	3.08	(δ-C7C8H32)(11)
87.	1253	1204	-	8.80	(δ-C24H41C25)(27)
86.	1246	1197	-	77.23	(δ-C4H34C11)(21)-(δ-C5H33C10)(14)-(δ-N2H31N3)(12)
85.	1234	1186	-	6.31	(δ-C24H41C25)(12)-v(C9C12)(10)
84.	1212	1164	1175	6.74	(δ-H44O6C30)(78)
83.	1204	1157	-	204.38	(δ-C15H37C19)(25)-(δ-C18H38C19)(20)
82.	1178	1132	1135	0.72	(δ-H45O6C30)(93)
81.	1165	1119	-	9.99	v(N2N3)(18)-(δ-Ph <sub>2</sub> )(16)v(C13N20)(13)
80.	1160	1115	1103	324.57	(δ-C11H36C14)(34)-(δ-C4H34C11)(17)
79.	1143	1098	-	11.38	(δ-C18H40C22)(22)-(δ-C21H39C22)(17)v(C15C19)(13)
78.	1135	1091	-	201.07	v(N2N3)(27)-(δ-C5H33C10)(11)(δ-Ph <sub>2</sub> )(11)
77.	1118	1074	1061	84.17	(δ-C28H43S1)(34)(δ-C25H42C27)(29)-v(C27C28)(10)
76.	1086	1043	-	36.79	v(C25C27)(3)-(δ-C28H43S1)(16)
75.	1077	1035	-	23.19	(δ-C5H33C10)(16)(δ-Ph <sub>2</sub> )(16)-v(C5N23)(14)
74.	1072	1030	1027	84.26	v(C30O6)(76)
73.	1045	1004	-	50.59	(δ-Th)(17)-v(S1C24)(14)v(C8C24)(12)-(δ-C24H41C25)(11)
72.	1024	984	974	0.33	(δ-Ph <sub>1</sub> )(49)v(C18C19)(11)
71.	1008	968	-	0.45	(γ-C11C13C14H36)(53)-(γ-C4C11C14H34)(32)
70.	1005	966	-	26.02	(γ-C12C7H35H32)(60)-(γ-C7C9C12H35)(24)
69.	966	928	929	9.44	(γ-C5C10H33)(78)(τ-Ph <sub>2</sub> )(10)
68.	963	925	-	1.17	(γ-C9C21C22H39)(44)-(γ-C21C18C22H40)(40)
66.	945	908	912	15.62	v(C13N20)(15)-v(C5N23)(14)-(δ-Ph <sub>2</sub> )(10)

65.	923	887	-	1.80	( $\gamma$ -C25C27C28H42)(43)-( $\gamma$ -C24C25C27H41)(31)
64.	894	859	864	19.38	( $\delta$ -C12H35C7)(13)
63.	888	853	847	8.68	( $\gamma$ -C7C9C12H35)(47)-( $\tau$ -H32C7C8N2)(17)
61.	864	830	832	13.98	( $\gamma$ -C4C11C14H34)(46)( $\gamma$ -C11C13C14H36)(23)
60.	860	826		9.44	( $\delta$ -Th)(43)v(S1C28)(38)
59.	858	824	823	5.68	( $\gamma$ -C24C25C27H41)(46)( $\gamma$ -C25C27C28H42)(13)( $\gamma$ -S1C27C28H43)(13)
58.	842	815	-	32.08	( $\delta$ -N20O16O26)(34)( $\delta$ -N23O17O29)(26)( $\delta$ -Ph <sub>2</sub> )(12)
56.	821	789	-	6.87	( $\gamma$ -C15C18C19H38)(47)( $\gamma$ -C9C15C19H37)(26)
55.	795	764	742	1.11	v(O6C18)(14)( $\delta$ -C12H35C7)(11)-( $\delta$ -C19C9C15)(10)
54.	760	730	732	0.01	( $\gamma$ -C5O17O29N23)(47)-( $\gamma$ -N23C10C4C5)(16)( $\gamma$ -C13O26O16N20)(15)
53.	751	722	-	5.46	v(S1C28)(18)-v(S1C24)(11)
52.	749	720	-	7.31	( $\delta$ oopC10C13C14N20)(26)-( $\tau$ -Ph <sub>2</sub> )(15)
49.	727	699	694	19.81	( $\tau$ -Ph <sub>1</sub> )(22)-( $\tau$ -H31N3C4C5)(20)( $\gamma$ -N2C4N3H31)(17)( $\tau$ -C8N2N3H31)(13)
48.	717	689	-	20.30	( $\gamma$ -S1C27C28H43)(22) -( $\gamma$ -C25C27C28H42)(10)
47.	711	683	-	60.24	$\tau$ (H31N3C4C5)(23)-( $\gamma$ -N2C4N3H31)(19)-( $\gamma$ -S1C27C28H43)(15)
45.	692	665		3.29	( $\tau$ -Ph <sub>2</sub> )(47)-( $\gamma$ -N3C5C11C4)(23)
44.	674	648	634	5.06	( $\gamma$ -C7N2C24C8)(18)
41.	601	577	581	12.17	v(S1C24)(14)( $\delta$ -Th)(12)( $\gamma$ -C7N2C24C8)(10)
39.	570	548	553	31.10	( $\tau$ -Th)( 23)-( $\tau$ -Th)(11)
38.	553	531	542	18.19	( $\tau$ -Th)(28)( $\delta$ -C18O6C30)(16)( $\delta$ -Ph <sub>1</sub> )(12)
37.	533	510	509	7.00	( $\gamma$ -O6C19C22C18)( 24)-( $\gamma$ -C12C15C 21C9)(16)-( $\tau$ -Ph <sub>1</sub> )(16)
36.	528	507	-	5.87	( $\delta$ -O26C13N20)(23)-( $\delta$ -O17C5N23)(10)-( $\gamma$ -O6C19C22C18)(10)
35.	525	504	-	6.62	( $\tau$ -Ph <sub>2</sub> )(24)( $\gamma$ -C10C14C13N20)( 21)-( $\gamma$ -C5C11C4N3)(20)-( $\tau$ -Ph <sub>2</sub> )(18)
34.	486	467	469	12.96	( $\tau$ -Th)(28)( $\tau$ -Th)(21)-( $\gamma$ -C8S1C25C24)(16)
33.	467	449	454	8.96	( $\delta$ -C18O6C19)(13)( $\delta$ -Ph <sub>1</sub> )(13)( $\delta$ -C18O6C30)(12)

<sup>a</sup> abbreviations: v - stretching;  $\delta$  - in-plane deformation;  $\gamma$  - out-of-plane deformation;  $\tau$  - torsion; as - asymmetric; s - symmetric; Ph<sub>1</sub> - methoxy substituted benzene ring; Ph<sub>2</sub> - dinitro substituted benzene ring; Th - thiophene ring; % of PED is given in brackets; IR<sub>int</sub> - IR intensity.

**Table 6**

Comparison between calculated and experimental <sup>1</sup>H and <sup>13</sup>C NMR chemical shifts  $\delta$  (ppm) for compound **3** in CDCl<sub>3</sub> as the solvent at (25°C).

Atom no.	Exp. <sup>1</sup> H NMR	Calcd <sup>1</sup> H NMR	Atom no.	Exp. <sup>13</sup> C NMR	Calcd <sup>13</sup> C NMR
H-31(s)	11.43	11.83	C-18	160.77	161.04
H-32(d)	7.18 ( <i>J</i> = 16.2 Hz)	7.12	C-8	150.25	153.78
H-33(d)	9.08 ( <i>J</i> = 2.4Hz)	9.37	C-13	144.28	141.43
H-34(d)	8.08 ( <i>J</i> = 9.6Hz)	8.08	C-4	142.2	141.39
H-35(d)	6.76 ( <i>J</i> = 16.2 Hz)	6.67	C-24	138.39	137.78
H-36(dd)	8.24 ( <i>J</i> = 9.5Hz, <i>J'</i> = 2.4Hz)	8.17	C-12	134.98	134.12
H-37,39(d)	7.56 ( <i>J</i> = 8.7 Hz)	7.52	C-5	132.26	131.55

H-38,40(d)	6.90 ( $J = 8.7$ Hz)	6.91	C-9	130.12	130.32
H-42(m)	7.43	7.63	C-28	128.61	127.79
H-44,45,46(s)	3.84	3.85	C-25	127.71	126.15
			C-15	126.61	125.9
			C-27	126.07	125.17
			C-14	125.55	124.88
			C-21	123.64	123.28
			C-10	120.89	119.65
			C-19	116.92	115.19
			C-22	114.84	113.33
			C-11	113.69	111.68
			C-30	55.66	41.24

s = singlet; d = doublet; dd = double doublet; m = multiplet

**Table 7**  
Selected TD-DFT excitations and approximate assignments for compound **3**.

Excitation energy (eV)	Experimental wavelength(nm)	Calculated wavelength(nm)	Oscillator strength ( $f$ )	Major transition and expansion coefficient	Assignments
In gas phase					
3.4083	-	364	1.0036	H(110) $\rightarrow$ L(111) (0.62053)	$\pi \rightarrow \pi^*$
3.9094	-	317	0.5939	H(110) $\rightarrow$ L+1(112) (0.58181)	$\pi \rightarrow \pi^*$
4.5348	-	273	0.2194	H-7(103) $\rightarrow$ L+1(112) (0.44561)	$\pi \rightarrow \pi^*$
5.5139	-	225	0.0875	H-8(102) $\rightarrow$ L(111) (0.31611)	$\pi \rightarrow \pi^*$
5.9033	-	210	0.1431	H-6(103) $\rightarrow$ L+1(112) (0.36009)	$\pi \rightarrow \pi^*$
In solvent dichloromethane (DCM)					

3.2411	421	382	1.1228	H(110) → L(111) (0.62053)	$\pi \rightarrow \pi^*$
3.7273	334	333	0.6341	H(110) → L+1(112) (0.52505)	$\pi \rightarrow \pi^*$
4.3628	278	284	0.2560	H-1(109) → L(111) (0.42107)	$\pi \rightarrow \pi^*$
5.3706	233	231	0.1239	H-6(104) → L(111) (0.36421)	$\pi \rightarrow \pi^*$
5.1740	219	215	0.1101	H-3(107) → L(111) (0.54783)	$\pi \rightarrow \pi^*$
In solvent ethanol					
3.2459	417	382	1.0872	H(110) → L(111) (0.62116)	$\pi \rightarrow \pi^*$
3.7210	331	333	0.6460	H(110) → L+1(112) (0.57350)	$\pi \rightarrow \pi^*$
4.3637	273	284	0.2518	H-1(109) → L(111) (0.42290)	$\pi \rightarrow \pi^*$
5.3610	230	231	0.1260	H-6(104) → L(111) (0.38547)	$\pi \rightarrow \pi^*$
5.1704	217	215	0.0944	H-3(107) → L(111) (0.44398)	$\pi \rightarrow \pi^*$

**Table 8**

Second order perturbation theory analysis of Fock matrix in NBO basis for selected donor (Lewis) and acceptor (non-Lewis) orbitals.

Donor( <i>I</i> )	Type	Acceptor( <i>J</i> )	Type	( $E^2$ ) <sup>a</sup> (kcal/mol)	E( <i>j</i> )-E( <i>i</i> ) <sup>b</sup> (a.u)	F( <i>ij</i> ) <sup>c</sup> (a.u)
N2-C8	$\pi$	C7-C12	$\pi^*$	10.88	0.38	0.058
N3-C4	$\pi$	N2-C8	$\pi^*$	16.90	0.36	0.073
C5-C10	$\pi$	N23-O29	$\pi^*$	30.89	0.15	0.066
		N3-C4	$\pi^*$	34.65	0.23	0.087
C7-C12	$\pi$	C9-C15	$\pi^*$	11.93	0.30	0.057
		N2-C8	$\pi^*$	19.88	0.27	0.067
C9-C15	$\pi$	C21-C22	$\pi^*$	20.00	0.28	0.068
		C18-C19	$\pi^*$	17.95	0.27	0.062
		C7-C12	$\pi^*$	17.80	0.29	0.067
C11-C14	$\pi$	N3-C4	$\pi^*$	32.70	0.22	0.085
C18-C19	$\pi$	C21-C22	$\pi^*$	15.46	0.30	0.061
		C9-C15	$\pi^*$	22.78	0.29	0.074
C21-C22	$\pi$	C18-C19	$\pi^*$	21.04	0.28	0.070
		C9-C15	$\pi^*$	16.15	0.29	0.063
C24-C25	$\pi$	C27-C28	$\pi^*$	14.74	0.30	0.061
C27-C28	$\pi$	C24-C25	$\pi^*$	16.13	0.29	0.064
C7-H32	$\sigma$	C8-C24	$\sigma^*$	4.85	0.96	0.061
		C12-H35	$\sigma^*$	4.33	0.98	0.058
C12-H35	$\sigma$	C7-H32	$\sigma^*$	4.74	0.99	0.061
C21-H39	$\sigma$	C18-C22	$\sigma^*$	4.02	1.07	0.059

C25-H41	$\sigma$	S1-C24	$\sigma^*$	4.82	0.74	0.053
C25-C27	$\sigma$	C8-C24	$\sigma^*$	4.72	1.12	0.065
C27-H42	$\sigma$	S1-C28	$\sigma^*$	4.17	0.76	0.050
S1	$n_2$	C24-C25	$\pi^*$	20.53	0.27	0.067
		C27-C28	$\pi^*$	21.56	0.27	0.070
N2	$n_1$	N3-H31	$\sigma^*$	8.56	0.84	0.087
		C8-C24	$\sigma^*$	11.25	0.87	0.028
O6	$n_1$	C18-C19	$\sigma^*$	7.58	1.10	0.082
O6	$n_2$	C18-C19	$\pi^*$	32.21	0.34	0.099
O17	$n_1$	N3-H31	$\sigma^*$	4.60	1.21	0.067
		C5-N23	$\sigma^*$	6.33	1.07	0.075
O16	$n_1$	C13-N20	$\sigma^*$	4.39	1.09	0.063
		N20-O26	$\sigma^*$	2.38	1.21	0.048
O26	$n_1$	C13-N20	$\sigma^*$	4.44	1.09	0.063
		O16-N20	$\sigma^*$	2.41	1.21	0.049
O29	$n_1$	C5-N23	$\sigma^*$	4.61	1.09	0.065
		O17-N23	$\sigma^*$	2.13	1.18	0.045

<sup>a</sup> Energy of hyper conjugative interactions(stabilization energy)

<sup>b</sup> Energy difference between donor  $i$  and acceptor  $j$  NBO orbitals.

<sup>c</sup> Fock matrix element between ( $i$ ) and ( $j$ )NBO orbitals.

**Table 9**

Calculated  $E_{\text{HOMO}}$ ,  $E_{\text{LUMO}}$ , energy band gap ( $E_{\text{H}} - E_{\text{L}}$ ), chemical potential ( $\mu$ ), electronegativity ( $\chi$ ), global hardness ( $\eta$ ), global softness ( $S$ ) and global electrophilicity index ( $\omega$ ) (in eV) for reactants **1**, **2**, product **3** at B3LYP/6-31G (d, p) level.

	$E_{\text{HOMO}}$	$E_{\text{LUMO}}$	$E_{\text{L}} - E_{\text{H}}$	$\chi$	$\mu$	$\eta$	$S$	$\omega$
Reactant ( <b>1</b> )	-5.823	-2.014	-3.809	3.918	-3.918	1.904	0.263	4.031
Reactant ( <b>2</b> )	-6.667	-2.748	-3.918	4.708	-4.708	1.959	0.255	5.656
Product ( <b>3</b> )	-5.551	-2.694	-2.857	4.122	-4.122	1.482	0.274	5.732

**Table 10**

Selected electrophilic reactivity descriptors ( $f_k^+$ ,  $s_k^+$ ,  $\omega_k^+$ ) and nucleophilic reactivity descriptors ( $f_k^-$ ,  $s_k^-$ ,  $\omega_k^-$ ) of reactants **1**, **2** and product **3** using Hirshfeld atomic charges.

Sites	$f_k^+$	$f_k^-$	$s_k^+$	$s_k^-$	$\omega_k^+$	$\omega_k^-$
Reactant( <b>1</b> )						
C9	0.147066	0.049022	0.038678	0.012893	0.592823	0.197608
C11	0.025492	-0.105413	0.006704	-0.02772	0.102758	-0.42492
C12	0.01850	-0.092769	0.004866	-0.0244	0.074574	-0.37396
Reactant( <b>2</b> )						
N16	-0.035248	-0.143794	-0.00899	-0.03667	-0.19936	-0.8133
N18	-0.061053	-0.183607	-0.01557	-0.04682	-0.34532	-1.03848
Product( <b>3</b> )						
C7	-0.011387	-0.069493	-0.00312	-0.01904	-0.06527	-0.39833
C8	0.0878479	0.017028	0.02407	0.004666	0.503545	0.097604

C12	0.0019988	-0.088606	0.000545	-0.02428	0.011458	-0.50789
-----	-----------	-----------	----------	----------	----------	----------

**Table 11**

Dielectric constant ( $\epsilon$ ) for solvents, dipole moment ( $\mu_0$ ) (Debye), polarizability ( $\alpha_0$ ) ( $10^{-24}$  esu), anisotropy of polarizability ( $\Delta \alpha$ ) ( $10^{-24}$  esu) and calculated first static hyperpolarizability ( $\beta_0$ ) ( $10^{-30}$  esu) for compound **3**.

Medium	$\epsilon$	$\mu_0$	$\alpha_0$	$\Delta \alpha$	$\beta_0$
vacuum	-	11.22	-26.68	2.15	8.36
DCM	4.90	13.16	-26.97	2.91	9.79
ethanol	24.30	13.36	-27.00	2.45	9.93

**Table 12.** Thermodynamic properties of compound **3** at different temperatures.

Temperature (K)	$H_m^0$ (kcal/mol)	$C_{P,m}^0$ (cal/mol-K)	$S_m^0$ (cal/mol -K)
<b>100</b>	215.136	50.54	113.827
<b>200</b>	220.734	78.471	152.902
<b>298.15</b>	229.040	107.367	187.102
<b>400</b>	240.573	135.053	220.761
<b>500</b>	254.420	157.711	252.008
<b>600</b>	270.301	175.85	281.275

FIGURE 10

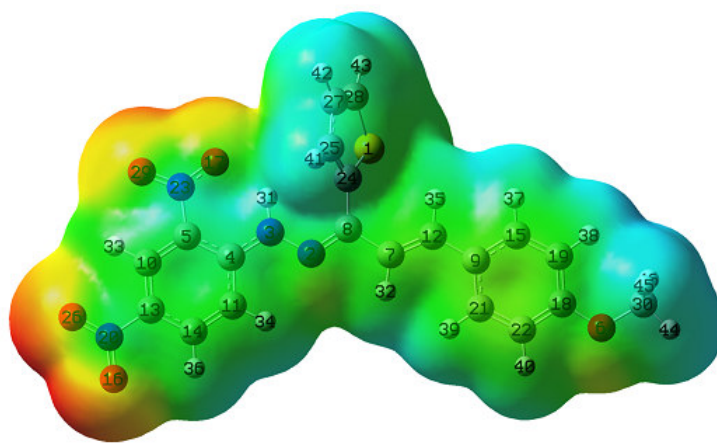
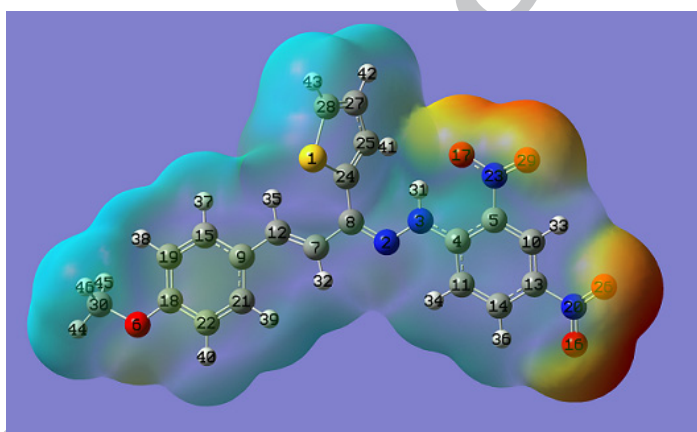


**Fig.10.** Molecular electrostatic potential surface (MEP) of the compound **3** at B3LYP/6-31G (d,p) level of theory. (For interpretation of the references to colour in this figure legend, the reader is referred to the web version of this article).

**GRAPHICAL ABSTRACT**

Quantum chemical calculations have been performed by DFT level of theory using B3LYP functional and 6-31G (d, p) as basis set using Gaussian 09 software package.



**HIGHLIGHTS**

- The structure of compound **3** was characterized by IR,  $^1\text{H}$  NMR,  $^{13}\text{C}$  NMR, UV-Vis. spectroscopy and single crystal X-ray diffraction.
- The wave numbers are assigned using PED analysis.
- Various hyper-conjugative interactions were analyzed by NBO analysis.
- The geometrical parameters are in agreement with XRD data.
- Weak intra-molecular interactions and ellipticity was analyzed by AIM approach